Binuclear Metallomacrocyclic M^{II}-Xanthate Complexes With Cu^{II}, Ni^{II} and Zn^{II} Holding Pendent Amido Groups in the Ligand Backbone: Synthesis, Characterization and DFT study

Abstract

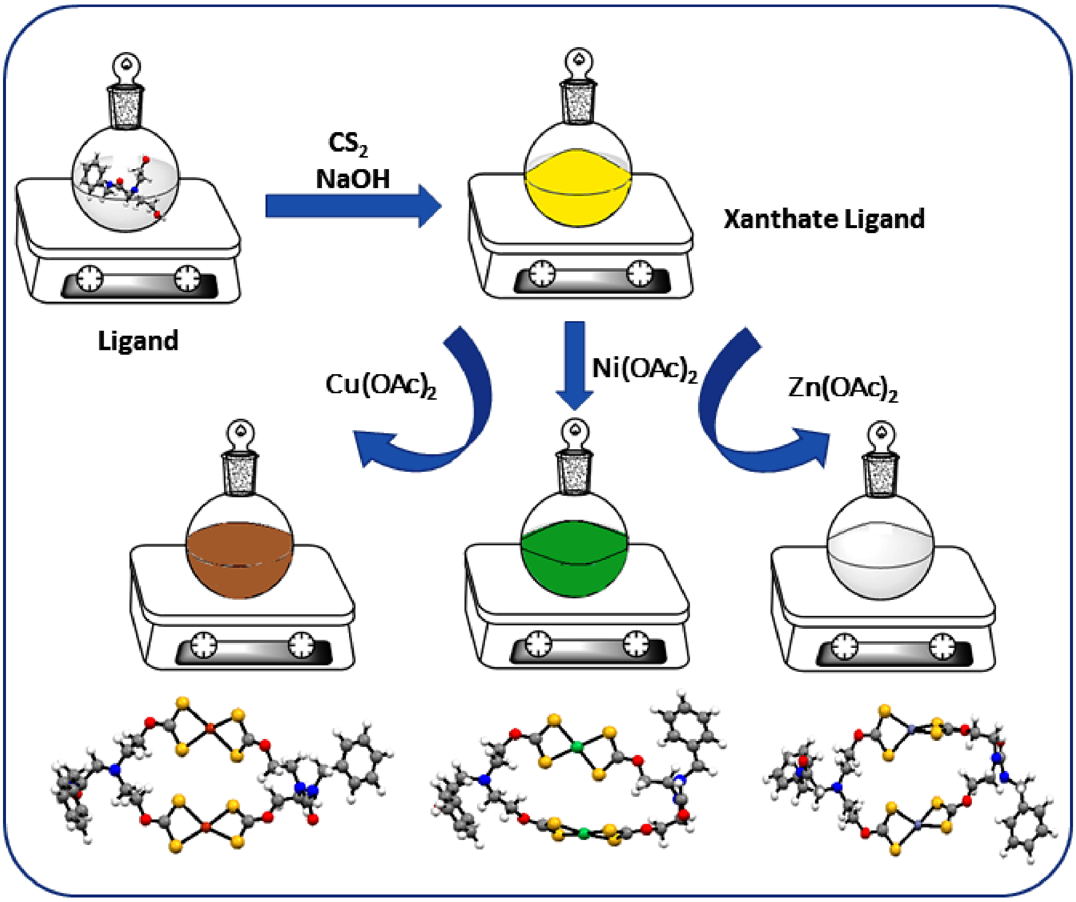

A new series of chiral/achiral diol- ligand precursors N-benzyl-2-(bis(2-hydroxyethyl)amino)acetamide (**L^1**), (S)-2-(bis(2-hydroxyethyl)amino)-N-(1-phenylethyl)acetamide (**L^2**), (R)-2-(bis(2-hydroxyethyl)amino)-N-(1-phenylethyl)acetamide (**L^3**) and their ensuing binuclear metallamacrocyclic xanthate complexes of type [M$^{II}{}_2$-μ^2-bis-{(κ^2S,S-$S_2COCH_2CH2)_2N(CH_2CONH(CH(G)Ph)$)}] {G=H, M= Cu^{II} **1**, G=CH_3, M= Cu^{II} S-**2**, G=CH_3, M= Cu^{II} R-**3**, G=H, M= Ni^{II} **4**, G=CH_3, M= Ni^{II} S-**5**, G=CH_3, M= Ni^{II} R-**6**, G=H, M= Zn^{II} **7**, G=CH_3, M= Zn^{II} S-**8** and G=CH_3, M= Zn^{II} R-**9}** holding pendent amido functional groups in the ligand backbone have been efficiently synthesized and characterized by the relevant spectroscopic (^{1}H, ^{13}C, HRMS, UV–visible absorption, IR) methods. The unprecedented molecular structure of ligand precursor(R)-2-(bis(2-hydroxyethyl)amino)-N-(1-phenylethyl)acetamide (L^3) has been determined by single crystal X-ray study, which further enlightened the packing patterns of molecules in the solid state. A DFT level calculation has been performed on all the diol ligand precursors (**L^1-L^3**) and M^{II}-xanthate complexes (**1, S-2, R-3, 4, S-5, R-6, 7, S-8, R-9**). The UV-visible absorption spectral study along with magnetic susceptibility measurements ascertained distorted square-planar geometry around Cu^{II} and Ni^{II} centres and distorted tetrahedral geometry around Zn^{II} centres in their respective complexes which is consistent with their optimized geometry at B3LYP/LanL2DZ level. Amongst the investigated compounds, Cu^{II} complexes **1**, **S-2**, **R-3** gave HOMO-LUMO energy band gaps in the range of 0.725-0.732 eV and demonstrate their semiconducting nature. The mapping of molecular electrostatic potential (MESP) of all the complexes revealed that positive charges are mainly accumulated amidic NH whereas negative charges are localized at amidic CO. This shows the potentials of these molecules to involve in an effective H-bonding interactions in the biological systems.

8.1 Introduction

The self-assembly processes occurring in nature have inspired synthetic chemists to engineered such structures at the molecular level.[1] The design and synthesis of such discrete molecular structures with diverse sizes and shapes has recently attracted great interest, but control over the arrangements of molecular fragments to obtain a particular product is still a challenge to synthetic chemists.[2] In this regard, metal-directed self-assembly process has emerged as one of the powerful synthetic technology for the formation of multi-dimensional structural motifs that possess interesting physico-chemical properties.[3]

Although, dithiocarbamates ligands with their ability to demonstrate a variable mode of binding and to stabilize the diverse oxidation states of various transition/ non-transition metal ions, have been competently utilized in the process of metal directed self-assembly, leading to a wide variety of discrete molecular structures such as metallomacrocyclic, [4-6] catenanes,[7] cavitands,[8] cryptands,[9] and container molecules.[10] However, in spite of the ready availability of xanthate ligands bearing functionalized backbone, isostructural xanthate ligands have scarcely been investigated in the metal directed self-assembling process, which underlines their synthetic challenges.

In particular, in the light of high degree of potency and selectivity of a wide range of natural products bearing macrocyclic motifs [11] in medicinal chemistry, synthetic chemists are enthused to discover a broader use of binuclear macrocyclic motifs in therapeutics. In recent times, our lab has examined in vitro cytotoxic activity of a number of 1,1-dithio based metallomacrocyclic complexes and some of them evidently showed remarkable activity against human hepatoma and neuroblastoma cell lines. [6, 12] Reports suggests that the sulfur atoms in the molecules as donor sites play various role viz. as chemoprotectants in chemotherapy, to modulate cisplatin nephrotoxicity and in transporting the molecule to the targets as well as protect against untimely reaction with biomolecules. [13]

The very limited literature reports on the metal-xanthate macrocyclic complexes [14] and their fascinating physio-chemical properties motivated us to carry out the synthesis and structural characterization of new copper(II), nickel(II) and zinc(II) complexes of xanthate ligands. The macrocycles holding flexible linkers would expand and change the size of the ring cavity and for selective binding with inorganic, organic small molecules and metal ions. Such compounds are anticipated to find potential applications in the area of analytical chemistry, physical chemistry, environmental science, synthetic organic chemistry and biochemistry.

This section reports on a facile synthesis of chiral diol ligand precursors and their corresponding binuclear metallamacrocyclic complexes [M^{II}_2-μ^2-bis-{(κ^2S,S-$S_2COCH_2CH2)_2N(CH_2CONH(CH(G)Ph))$}] {G=H, M= Cu^{II} **1**, G=CH_3, M= Cu^{II} S-**2**, G=CH_3, M= Cu^{II} R-**3**, G=H, M= Ni^{II} **4**, G=CH_3, M= Ni^{II} S-**5**, G=CH_3, M= Ni^{II} R-**6**, G=H, M= Zn^{II} **7**, G=CH_3, M= Zn^{II} S-**8** and G=CH_3, M= Zn^{II} R-**9}** in a multicomponent single pot reaction involving diol, carbon disulphide and metal ions**.** All newly synthesized ligand precursors (L^1-L^3) and their corresponding mettallomicrocyclic xanthate complexes (**1**, S-**2**, R-**3**, **4**, S-**5**, R-**6**, **7**, S-**8** and R-**9)** are characterized by relevant spectroscopic methods and microanalysis. Single crystal X-ray diffraction study of ligand L^3 has been performed to elucidate the molecular structure and investigate packing pattern in solid state. A DFT level calculations have been carried out to reinforce the experimental outcomes.

8.2 Experimental

8.2.1 Materials and measurements

All solvents were purchased from the commercial sources and were freshly distilled prior to use. All the reagents such as $Cu(OAc)_2 \cdot H_2O$, $Ni(OAc)_2.4H_2O$, $Zn(OAc)_2 \cdot H_2O$ and CS_2 were purchased from Merck and Sigma-Aldrich Chemicals Limited, these were used without further purification. Elemental analyses (C, H, N, S) were carried out on a Perkin-Elmer 2400 analysers. Thin Layer Chromatography was performed on Merck 60 F254 Aluminium coated plates. FT-IR spectra were recorded in the 4000-400 cm^{-1} range using a Perkin-Elmer FT-IR spectrometer as KBr pellets. The ^{1}H and ^{13}C NMR spectra of relevant compounds were obtained on a Bruker AV-III 400 MHz spectrometer in spectrometer with DMSO-d_6 as solvent and TMS as internal standard. UV-visible spectra were recorded on a JASCO V-730 UV-visible spectrophotometer. High resolution mass spectrometry (HRMS) was carried out in ESI positive ionization mode using Agilent Technologies, model – 6545 Q-TOF LC/MS system by direct injection of 1 ppm sample solution at a flow rate of 20 μL/min. The following parameters were used for mass spectrometric analyses. Gas temperature was set at 320 ^{0}C with a flow rate of 8 L Min^{-1}; nebulizer pressure was set at 35 psig ; drying gas temperature was maintained at 350 ^{0}C with a flow rate of 11 L Min^{-1} ; capillary voltage and nozzle voltage were set at 3500 V and 1000 V respectively; fragmentor voltage and skimmer voltage were set at 175V and 65 V respectively and octopole RF peak was 750 V. Scan rate was maintained 3 spectra/s. Mass hunter software supplied by the manufacturer was used for data acquisition.

8.2.2 General synthetic procedure for the synthesis of diol ligand precursors (L^1, L^2 and L^3)

In a typical reaction, N-benzyl-2-iodoacetamide (0.578 g, 2.1 mmol), (S)-2-iodo-N-(1-phenylethyl)acetamide (0.608 g, 2.1 mmol) or (R)-2-iodo-N-(1-phenylethyl)acetamide (0.608 g, 2.1 mmol) was added in two portions to a solution of diethanolamine (2 00g, 2.0 mmol, d=1.09 g/cm^3) in 25 ml of CH_3CN containing 2.5 mmol of Na_2CO_3. The reaction mixture was reflux for 6-7 hours. The progress of the reaction was monitored by thin layer chromatography. The reaction mixture was cooled at room temperature and solvent was removed under vacuum by using rotary evaporator. Added 1-2 ml of distilled water to the solid residue and the crude product was extracted by using ethyl acetate. It was dried over Na_2SO_4 for 1 hours and the solvent was removed by rotator evaporator. The residue was column chromatographed to give off-white coloured thick liquid product of **L^1** and white-coloured solid products of **L^2** and **L^3** in 75-80 % yield.

8.2.3 General Synthetic procedure for the synthesis of M^{II}-xanthate complexes (1, S-2, R-3, 4, S-5, R-6, 7, S-8 and R-9)

Two equivalents of amide functionalized alcohol precursor *viz.* N-benzyl-2-(bis(2-hydroxyethyl)amino)acetamide (**L^1**) (0.252 g, 1.0 mmol), (S)-2-(bis(2-hydroxyethyl)amino)-N-(1-phenylethyl)acetamide (**L^2**) (0.266 g, 1.0 mmol) or (R)-2-(bis(2-hydroxyethyl)amino)-N-(1-phenylethyl)acetamide (**L^3**) (0.266 g, 1.0 mmol) was dissolved in 30 ml of acetonitrile containing NaOH (0.120 g, 3 mmol) and the mixture was stirred for 30 minutes. An excess amount of carbon disulfide (0.3 ml, 300 µl, 5 mmol) was added to this solution and the reaction mixture was continued to stir for 12 hr. The *in-situ* formation of corresponding xanthate ligand was monitored by a change in color from colorless to yellow. To this solution, $Cu(OAc)_2 \cdot H_2O$ (199.6 mg, 1 mmol) , $Ni(OAc)_2 \cdot 4H_2O$ (248.8 mg, 1 mmol) and $Zn(OAc)_2 \cdot H_2O$ (219.5 mg, 1 mmol) were added and the mixture was continued to stir for 6-7 hrs. The progress of reaction was monitored by thin layer chromatography. The reaction mixture was concentrated on rotatory evaporator leaving the residue. The residue was filtered, washed with distilled water (5ml × 2 times) followed by petroleum ether (5ml × 3 times) and dried under high vacuum to give the products in 80-90 % yield. The overall reaction is outlined in Scheme1. The solid products were stored under nitrogen and data were collected.

8.3 RESULTS AND DISCUSSION

8.3.1 Synthesis and Characterization

Three diol precursors viz. N-benzyl-2-(bis(2-hydroxyethyl)amino)acetamide (**L^1**), (S)-2-(bis(2-hydroxyethyl)amino)-N-(1-phenylethyl)acetamide (**L^2**) or (R)-2-(bis(2-hydroxyethyl)amino)-N-(1-phenylethyl)acetamide (**L^3**) were designed and synthesized conveniently by following Scheme 1. A single pot reaction involving self-assembly of **L^1**, **L^2** or **L^3** with CS_2 and Cu^{II}/ Ni^{II} or Zn^{II} metal ion in CH_3CN under basic condition affords access to a new series of binuclear metallamacrocyclic M^{II}-xanthate complexes $[M^{II}_2\text{-}\mu^2\text{-bis-}\{(\kappa^2S,S\text{-}S_2COCH_2CH_2)_2N(CH_2CONH(CH(G)Ph))\}]$ {G=H, M= Cu^{II} **1**, G=CH_3, M= Cu^{II} S-**2**, G=CH_3, M= Cu^{II} R-**3**, G=H, M= Ni^{II} **4**, G=CH_3, M= Ni^{II} S-**5**, G=CH_3, M= Ni^{II} R-**6**, G=H, M= Zn^{II} **7**, G=CH_3, M= Zn^{II} S-**8** and G=CH_3, M= Zn^{II} R-**9}**, (Scheme 2) holding pendent amido functional groups in the ligand backbone. A single pot multicomponent synthetic methodology involving several chemical operations simultaneously in a single container has distinctive advantages such as it reduces the purifications of the intermediate compounds, and it may eventually save valuable resources. After workup the products were obtained as brown (in case of Cu^{II}), green (in case of Ni^{II}) and white powder (in case of Zn^{II}) in 80–90% isolated yields. Besides N^{II}-xanthate complexes (**4**, *S*-**5**, *R*-**6**), all the complexes are soluble in the solvents of high nucleophilicity such as DMSO and DMF. All the binuclear M^{II}-xanthate complexes (**1**, S-**2**, R-**3**, **4**, S-**5**, R-**6**, **7**, S-**8** and R-**9)** appeared to be stable in the solid state and in solution over a period of days.

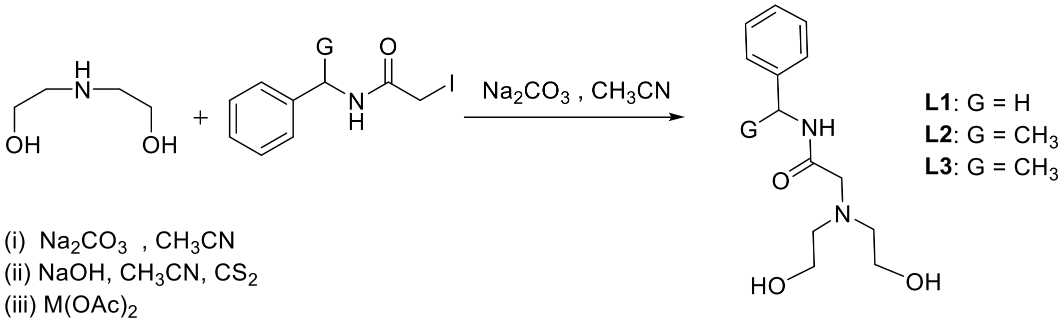

Scheme 1. General synthetic strategies adopted for the synthesis of amide functionalized ligand (L^1, S-L^2 and R-L^3).

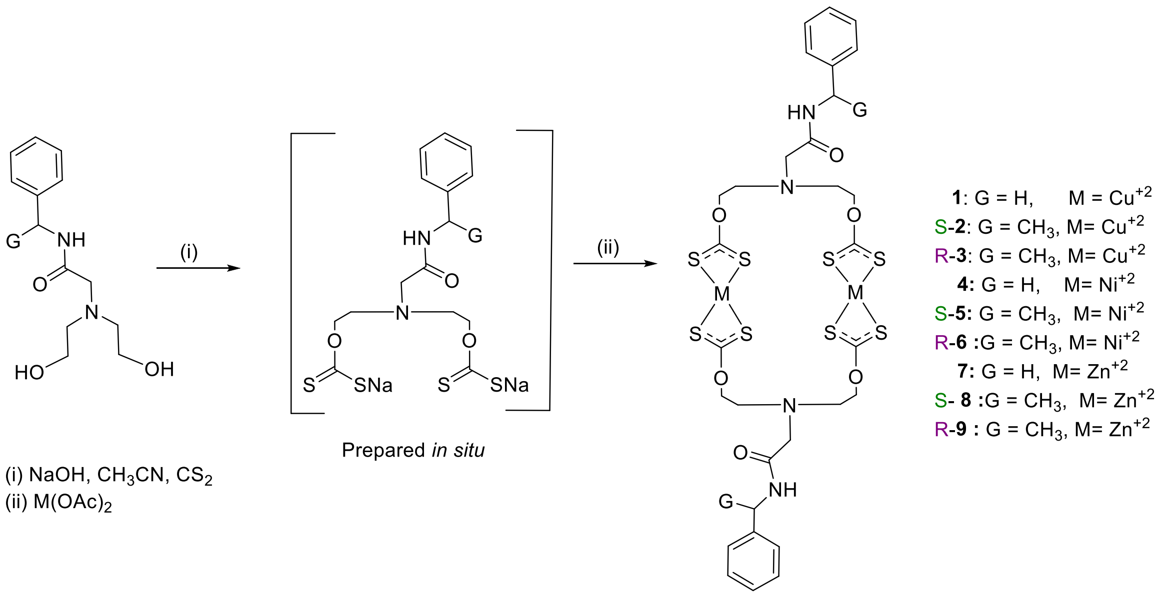

Scheme 2. General synthetic strategies adopted for the synthesis of amide functionalized binuclear metallamacrocyclic M^{II}-xanthate complexes (**1**, S-**2**, R-**3**, **4**, S-**5**, R-**6**, **7**, S-**8** and R-**9**).

The formulation and purity of ligands (L^1, L^2 and L^3) and ensuing binuclear metallamacrocyclic M^{II}-xanthate complexes (**1**, S-**2**, R-**3**, **4**, S-**5**, R-**6**, **7**, S-**8** and R-**9)** were ascertained by, IR, HRMS, NMR (^{1}H and ^{13}C) spectroscopy and elemental analysis. The microanalysis data (Table1) along with HRMS data (Table 2) confirms the composition of the products.

The HRMS analysis of one of the Cu^{II}-xanthate complex 1 is carried out in the negative ionization mode while other complexes are analysed in the positive ionization mode. The HRMS analysis of Cu^{II}-xanthate complexes 1 ($C_{30}H_{36}Cu_2N_4O_6S_8$), S-**2** ($C_{32}H_{40}Cu_2N_4O_6S_8$) and R-**3** ($C_{32}H_{40}Cu_2N_4O_6S_8$) shows peak at 928.9009 $[M-H]^-$, 958.9406 ($[M+H]^+$ and 958.9381 $[M+H]^+$ against calculated mass of 928.892 $[M-H]^-$, 958.9378 $[M+H]^+$ and 958.9378 $[M+H]^+$ with an error of 2.91 ppm, 2.91ppm and 0.31 ppm, respectively. Similary, composition of remaining complexes have been verified by their respective The HRMS analysis. The ^{1}H NMR spectrum of L^1, L^2, L^3 gave amidic NH signals in the range of 8.42-8.52 ppm apart from the signals due to aryl, methylene, methene and methyl fragments (Table 3). The ^{1}H signals corresponding to alcoholic OH groups in L^1, L^2, L^3 appeared in the region of 4.63-4.70 ppm whereas methylene (-CH_2O) signals are evidently appeared in the region of 3.38-3.47 ppm. ^{1}H NMR of L^1-L^3 are well supported by their corresponding ^{13}C NMR spectral study (Table 3). The NMR study of Ni^{II}-xanthate complexes (4, S-5, R-6) could not be performed due to their insolubility in common deuterated solvents including DMSO $d_{6.}$ However, all the diamagnetic Zn^{II}-xanthate complexes R-**6**, **7**, S-**8** have been satisfactorily characterized by their ^{1}H and ^{13}C NMR spectral study.

Notably, the disappearance of OH signals of diol ligand precursors in their ensuing Zn^{II}-xanthate complexes R-**6**, **7**, S-**8** and a considerable shifting in the ^{1}H NMR chemical shift of the methylene (-CH_2O) signals, compared to free diol precursors L^1-L^3, reinforce the formation of proposed structures as they are most sensitive to any chemical change at –OH functionality. Moreover, the ^{1}H NMR spectra of complexes 8 and 9 gave two methyl signals apparently due to chirality induced asymmetric benzylic carbons

Table 1. Micro-, mass- and IR analysis data for ligand (**L**[1]**, L**[2] and **L**[3]) and complexes (**1**, S-**2**, R-**3**, **4**, S-**5**, R-**6**, **7**, S-**8** and R-**9**).

Entry	Molecular Formula	Molecular Weight	Yield (%)	MP/BP (°C)	Elemental Analysis % Found (calculated)			IR data (KBr disc) υ_{max}/cm^{-1}
					C	H	N	
L[1]	$C_{13}H_{20}N_2O_3$	252	75	137	61.78 (61.88)	7.87 (7.99)	11.24 (11.10)	3307 (O-H), 3064 (C-H), 2940 (C-H), 1653 (C=O), 1535, 1453, 1076, 752, 699, 611.
L[2]	$C_{14}H_{22}N_2O_3$	266	89	145	63.18 (63.13)	8.56 (8.33)	10.78 (10.52)	3343 (O-H), 2952 (C-H), 1671 (C=O), 1519, 1446, 1373, 1279, 1227, 1132, 1080, 1013, 981, 901, 877, 766, 704, 610, 536.
L[3]	$C_{14}H_{22}N_2O_3$	266	90	146	63.19 (63.13)	8.49 (8.33)	10.72 (10.52)	3343 (O-H), 2952 (C-H), 2830 (C-H), 1671 (C=O), 1519, 1446, 1373, 1279, 1228, 1132, 1081, 1014, 981, 901, 877, 767, 705, 610, 353.
1	$C_{30}H_{36}Cu_2N_4O_6S_8$	932	85	>250	38.71 (38.65)	3.95 (3.89)	6.11 (6.01)	2929 (C-H), 2857 (C-H), 1603 (C=O), 1569, 1410, 1222, 1131, 1104, 1026 ν(CS_2), 771, 698, 637, 536.
S-2	$C_{32}H_{40}Cu_2N_4O_6S_8$	960	86	>250	40.15 (40.03)	4.29 (4.20)	5.90 (5.83)	2926 (C-H), 2852 (C-H), 1625 (C=O), 1555, 1248, 1135, 1022 ν(CS_2), 766, 700, 618, 542.
R-3	$C_{32}H_{40}Cu_2N_4O_6S_8$	960	85	>250	40.18 (40.03)	4.27 (4.20)	5.90 (5.83)	3029 (C-H), 1626 (C=O), 1432, 1245, 1134, 1022 ν(CS_2), 768, 699, 617, 539, 462.
4	$C_{30}H_{36}Ni_2N_4O_6S_8$	922	82	>250	39.79 (39.60)	4.02 (3.93)	6.16 (6.07)	2927 (C-H), 2855 (C-H), 1628 (C=O), 1569, 1415, 1132, 1052 ν(CS_2), 1002, 771, 699, 542
S-5	$C_{32}H_{40}Ni_2N_4O_6S_8$	950	83	>250	40.48 (40.43)	4.31 (4.24)	5.78 (5.89)	3091 (C-H), 2972 (C-H), 1625 (C=O), 1574, 1142, 1021 ν(CS_2), 701, 623, 542.
R-6	$C_{32}H_{40}Ni_2N_4O_6S_8$	950	85	>250	40.55 (40.43)	4.33 (4.24)	5.91 (5.89)	2975 (C-H), 2842(C-H), 1602 (C=O), 1453, 1420, 1132, 1023 ν(CS_2), 767, 681, 618, 538.
7	$C_{30}H_{36}Zn_2N_4O_6S_8$	935	90	>250	38.61 (38.50)	4.90 (3.88)	6.15 (5.99)	2983 (C-H), 2845(C-H), 1602 (C=O),1562, 1414, 1153, 1045 ν(CS_2), 1022, 959, 806, 645, 526, 474.
S-8	$C_{32}H_{40}Zn_2N_4O_6S_8$	963	89	>250	39.92 (39.87)	4.23 (4.18)	5.88 (5.81)	2953 (C-H), 2830 (C-H), 1672(C=O), 1639, 1560, 1415, 1156, 1132, 1080 ν(CS_2), 1044, 927, 767, 1015, 643, 535, 474.
R-9	$C_{32}H_{40}Zn_2N_4O_6S_8$	963	90	>250	39.95 (39.87)	4.26 (4.18)	5.90 (5.81)	3023 (C-H), 2830 (C-H), 1672(C=O), 1639, 1559, 1414, 1227, 1132, 1080 ν(CS_2), 1015, 902, 878, 767, 705, 643, 536, 490.

Table 2. HRMS spectral data for the M^{II}-xanthate complexes (**1**, S-**2**, R-**3**, **4**, S-**5**, R-**6**, **7**, S-**8** and R-**9**).

Compounds	Calc. Mass	Obs. mass	Error(ppm)	Compounds	Calc. Mass	Obs. mass	Error(ppm)
1	928.892 $[M-H]^-$	928.9009	9.58 (higher side)	**R-6**	948.9493 $[M+H]^+$	948.9481	1.26
S-2	958.9378 $[M+H]^+$	958.9406	2.91	**7**	932.9056 $[M+H]^+$	932.9032	2.57
R-3	958.9378 $[M+H]^+$	958.9381	0.31	**S-8**	960.9369 $[M+H]^+$	960.9364	0.52
4	958.8739 $[M+H]^+$	958.8656	8.65 (higher side)	**R-9**	946.9213 $[M+H]^+$	946.9225	1.26
S-5	948.9493 $[M+H]^+$	948.9481	1.26	-	-	-	-

Table 3. NMR spectral data for ligand (**L^1, L^2** and **L^3**) and complexes (**4**, S-**5**, R-**6**, **7**, S-**8** and R-**9**).

Entry	NMR Data (ppm)	
	^{1}H NMR (DMSO d_6)	**^{13}C NMR (DMSO d_6)**
L^1	8.52 (s, 1H, -N*H*CO); 7.20-7.33 (m, 5H, Ph); 4.63 (s, 2H, -O*H*); 4.31 (d, 2H, -CH_2Ph); 3.44-3.47 (t, 4H, -CH_2O); 3.17 (s, 2H, -CH_2CO); 2.57-2.60 (t, 4H, -CH_2N).	171.2, 143.8, 128.8, 127.6, 126.2, 59.3, 57.4, 49.7, 48.3, 42.5
L^2	8.40 (s, 1H, -N*H*CO); 7.19-7.34 (m, 5H, Ph); 4.92 (m, 1H, -CH); 4.65 (s, 2H, -O*H*); 3.38-3.45 (t, 4H, -CH_2O); 3.12 (s, 2H, -CH_2CO); 2.50-2.61 (m, 4H, -CH_2N); 1.35 (d, 3H, -CH_3).	171.1, 143.7, 128.7, 127.6, 126.2, 59.2, 57.3, 49.3, 48.7, 42.6, 21.7
L^3	8.42 (s, 1H, -N*H*CO); 7.19-7.34 (m, 5H, Ph); 4.92 (m, 1H, -CH); 4.70 (s, 2H, -O*H*); 3.46 (m, 4H, -CH_2O); 3.13 (s, 2H, -CH_2CO); 2.50-2.61 (m, 4H, -CH_2N); 1.36 (d, 3H, -CH_3).	170.1, 143.6, 129.0, 128.6, 127.5, 126.1, 58.7, 57.0, 48.8, 42.6, 21.7
7	8.55 (s, 2H, -N*H*CO); 7.20-7.35 (m, 10H, Ph); 4.32 (d, 2H, -CH_2Ph); 3.39 (m, 8H, -CH_2O); 3.11 (s, 2H, -CH_2CO); 2.57-2.60 (t, 8H, -CH_2N).	171.7, 146.1.8, 128.7, 127.3, 126.0, 59.1, 48.5
S-8	8.42 (s, 2H, -N*H*CO); 7.18-7.39 (m, 10H, Ph); 4.92 (m, 2H, -CH); 3.11-3.17 (m, 8H, -CH_2O); 3.10 (s, 4H, -CH_2CO); 2.57-2.59 (m, 8H, -CH_2N); 1.67 (d, 3H, -CH_3), 1.35 (d, 3H, -CH_3).	170.7, 145.1, 128.6, 127.0, 126.3, 59.1, 48.1, 42.6, 24.8, 23.0
R-9	8.42 (s, 2H, -N*H*CO); 7.19-7.35 (m, 10H, Ph); 4.92 (m, 2H, -CH); 3.44-3.46 (m, 8H, -CH_2O); 3.11 (s, 4H, -CH_2CO); 2.57-2.60 (m, 8H, -CH_2N); 1.63 (d, 3H, -CH_3), 1.35 (d, 3H, -CH_3).	170.6, 145.2, 128.7, 127.0, 126.3, 59.1, 48.1, 23.1

.

The IR spectra of diol precursors L^1-L^3 gave ν(OH) and ν(C=O) bands at ~ 3300 cm^{-1} ~ 1660 cm^{-1}, apart from the bands due to aromatic/ aliphatic groups. In the IR spectra of M^{II}-xanthate complexes (**1**, S-**2**, R-**3**, **4**, S-**5**, R-**6**, **7**, S-**8** and R-**9**), the appearance of new bands in the 1150-1021 cm^{-1} region, attributable to xanthate moiety, indicates the formation of corresponding xanthate complexes. The existence of only one band for ν(CSS) vibrations in 1080-1021 cm^{-1} region indicates the symmetrical behaviour of the bidentate xanthate moiety. Further, a medium to weak intensity ν(M-S) bands in the 637-462 cm^{-1} region appeared which is consistent with the literature repots.[15] In the spectra of all the complexes a broad, strong bands due to O-H stretching mode around 3400 cm^{-1} are associated with the hygroscopic nature of the complexes.

8.3.2 UV-Visible absorption study

The electronic absorption spectral study of the ligand precursors L^1-L^3 and their M^{II}-xanthate complexes (**1**, S-**2**, R-**3**, **4**, S-**5**, R-**6**, **7**, S-**8** and R-**9**) was performed in 10^{-4} M CH_3CN solution (Figure 1) and the relevant data is tabulated in the Table 3. Ligand precursors L^1-L^3 a single absorption band at ~ 260 nm, attributable to $\pi\rightarrow\pi^*$ transitions. All the M^{II}-xanthate complexes displayed three single sharp bands at ~ 270 nm, ~ 300 nm and ~ 400 nm (Figure 1, Table 4), attributable to intra-ligand $\pi\rightarrow\pi^*$, $n\rightarrow\pi^*$ and LMCT transitions, respectively. [12-16] Apart from the bands due to $\pi\rightarrow\pi^*$ and LMCT charge-transfer transitions, a broad band appears at ~ 640–644 nm which is attributed to d-d transition [16] in case of copper complexes **1**, S-**2**, R-**3**. (Figure 1)

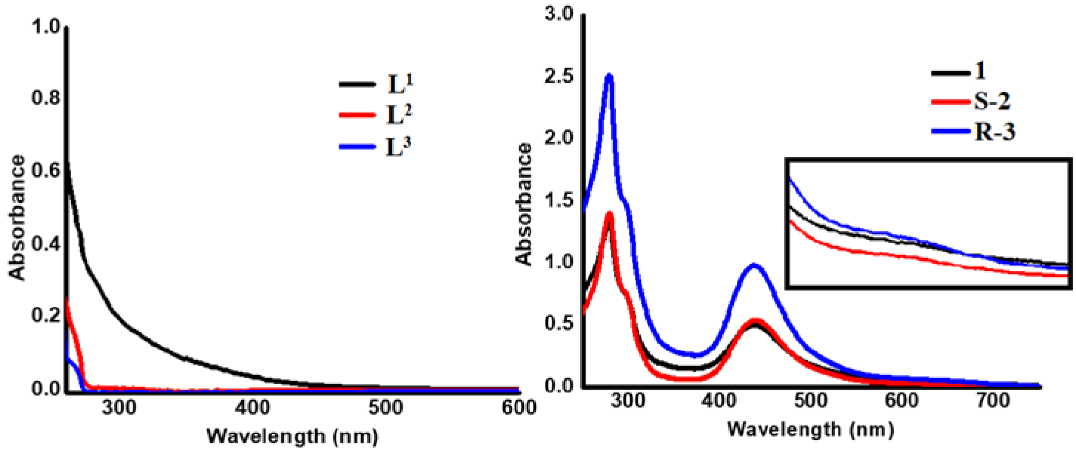

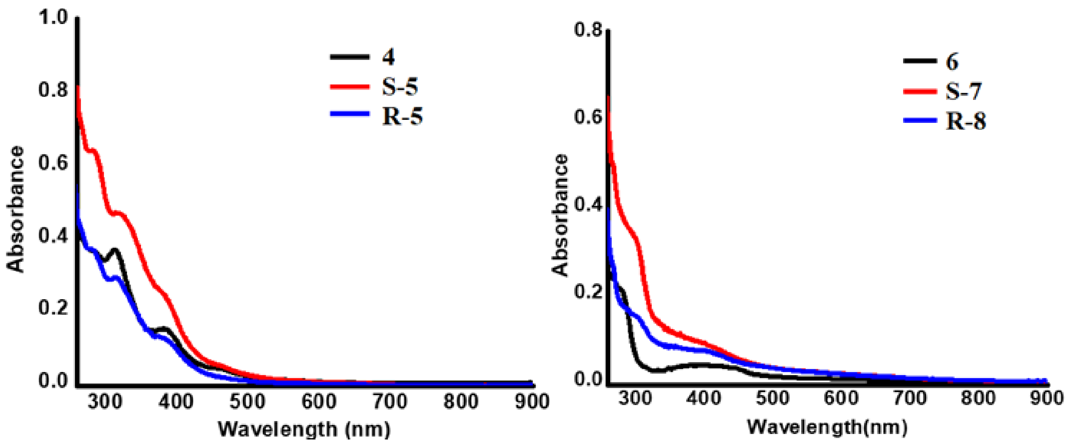

Figure 1. UV-visible absorption spectra of ligand precursors L1-L3 and their xanthate complexes **1**, S-**2**, R-**3**, **4**, S-**5**, R-**6**, **7**, S-**8** and R-**9** recorded at room temperature.

Table 4. UV-visible absorbance bands for of ligand precursors L1-L3 and their xanthate complexes **1**, S-**2**, R-**3**, **4**, S-**5**, R-**6**, **7**, S-**8** and R-**9** under investigation.

Entry	λ_{max} nm (10^{-4} M CH_3CN, ε L Mol^{-1} cm^{-1})	Magnetic Moment μeff (BM)
L1	265 (49815) π→ π*	-
L2	266 (13297) π→ π*	-
L3	266 (5603) π→ π*	-
1	277 (1312) π→ π*, 298 (1488) n→ π*, 438 (496) charge transfer, 644 (49) d-d transition.	1.83
S-2	278 (1400) π→ π*, 296 (755) n→ π*, 436 (539) charge transfer, 640 (223) d-d transition.	1.89
R-3	278 (2515) π→ π*, 296 (764) n→ π*, 436 (981) charge transfer, 644 (61) d-d transition.	1.88
4	282 (36408) π→ π*, 313 (36408) n→ π*, 384 (14732) charge transfer	**dia**
S-5	284 (35547) π→ π*, 315 (46112) n→ π*, 385 (23575) charge transfer	**dia**
R-6	283 (63797) π→ π*, 314 (29001) n→ π*, 386 (11575) charge transfer	**dia**
7	266 (23958) π→ π*, 300 (12568) n→ π*, 405 (3374) charge transfer	**dia**
S-8	269 (47305) π→ π*, 301 (31971) n→ π*, 402 (9084) charge transfer	**dia**
R-9	269 (24418) π→ π*, 303 (14587) n→ π*, 403 (7035) charge transfer	**dia**

Magnetic moment values, NMR studies and UV-visible absorption bands certainly suggest distorted square planar geometry around Ni^{II}/Cu^{II} centers and distorted tetrahedral environment around Zn^{II} centers in their corresponding M^{II}-

xanthate complexes [17-18] which is further verified by DFT calculation performed at B3LYP/ LanL2DZ level..

8.3.3 X-ray crystallographic study

Single crystals for X-ray analysis for L^3 was grown by slow evaporation of ethyl acetate solution at room temperature. The molecules of L^3 crystallized in triclinic P_1 space group. The X-ray crystal structure of this ligand L^3 shows two of the molecules of [$C_{28}H_{43}N_4O_6$] in its asymmetric unit. (Figure 2a) Information about data collection, refinement, and structure solution are recorded in (Table 5). There are two units in the unit cell (Figure 2b). Two molecules present in the asymmetric unit of L3, are connected through O1-H1a…O4 (1.974 Å) intermolecular hydrogen bonding interactions which is further extended towards a-axis by involving O2-H2…O5 (1.868 Å), forming a fascinating S-shaped 1D molecular architecture as shown in Figure 2(c).

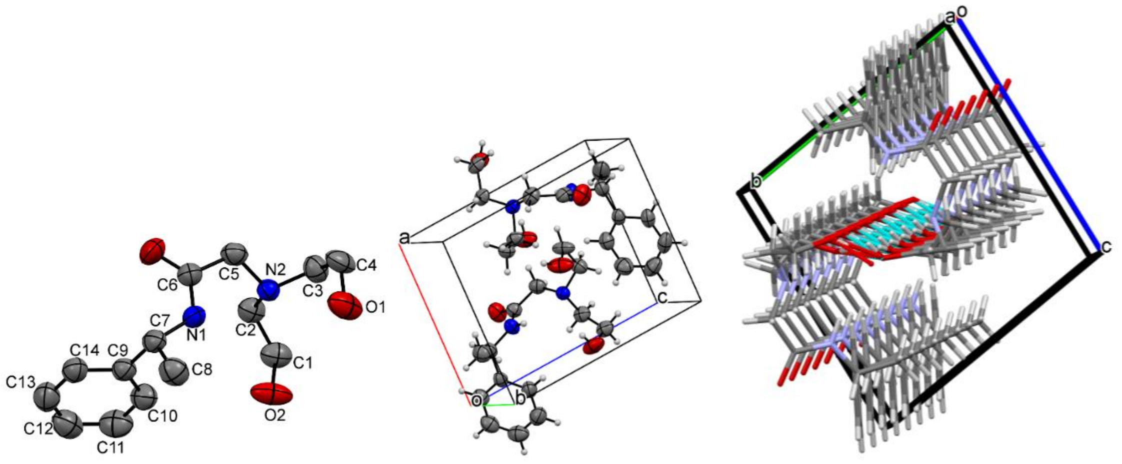

(a) **(b)** **(c)**

Figure 2. (a) Thermal ellipsoidal plot of ligand R-L^3 with atomic numbering, (b) presence of two molecules per unit cell. (c) overall molecules are stacked along *a* -axis through intermolecular hydrogen bonding interactions forming an infinite 1D molecular layer like symbol of doller.

Table 5. Crystal data and structure refinement for the compounds under investigation.

Identification code	**R-L^3**
Formula	$C_{28}H_{43}N_4O_6$
Formula weight	531.677
Temperature/K	293
Crystal system	triclinic
Space group	P1
a/Å	8.3825(7)
b/Å	9.4239(7)
c/Å	9.6353(8)

$\alpha/°$	81.431(7)
$\beta/°$	85.908(6)
$\gamma/°$	78.299(7)
Cell volume/$Å^3$	736.35(10)
Z	1
$\rho_{calc}g/cm^3$	1.199
μ/mm^{-1}	0.084
F(000)	287.1
Radiation	Mo Kα (λ = 0.71073)
2Θ range for data collection/°	6 to 58.58°
Index ranges	$-11 \leq h \leq 11$, $-12 \leq k \leq 12$, $-12 \leq l \leq 13$
Reflections collected	16102
Independent reflections	6819[R(int) = 0.0396]
Data/restraints/parameters	6819/3/349
Goodness-of-fit on F^2	1.109
Final R indexes [I>=2σ (I)]	R_1 = 0.0583, wR_2 = 0.1021
R indexes [all data]	R_1 = 0.1157, wR_2 = 0.1297
Larg. diff. peak/hole /$eÅ^{-3}$	0.26/-0.24
Flack parameter	-2.8(16)

8.3.4 Theoretical Investigations.

8.3.4.1 Density functional theory calculations

A DFT level calculations and full geometry optimizations has been performed on all ligand (L^1, L^2 and L^3) and their complexes with Cu^{II}, Ni^{II}, Zn^{II} (**1**, S-**2**, R-**3**, **4**, S-**5**, R-**6**, **7**, S-**8**, R-**9**) by using B3LYP/LanL2DZ basis sets. The optimized structures for the minimum energy conformation of these complexes are presented in (Figure 3). Gaussian 6.0 program suite [19] has been used for calculations and molecular orbitals were generated by GaussView 3.0 program. The use of analogues calculations have resulted appreciable results for bulky and mettallomicrocyclic structures.[20] Moreover, the calculated HOMO-LUMO gaps (Table 6) are comparable to the experimental UV-visible absorption data and validate the computed data as well as optimized structures.

Table 6. Summary of Computational study performed on all ligand (L^1, S-L^2 and R-L^3) and their complexes with Cu^{II}, Ni^{II}, Zn^{II} (**1**, S-**2**, R-**3**, **4**, S-**5**, R-**6**, **7**, S-**8** and R-**9**).

Code	Energy (Hatree)	HOMO (ev)	LUMO(ev)	Band Gap (ev)	Theoretical λ_{max} value (experimental λ_{max} value) nm
L^1	-842.598	-5.9250	-0.2209	5.704	217(265)
S-L^2	-881.915	-5.9198	-0.1877	5.732	216(266)
R-L^3	-881.917	-5.7930	-0.1913	5.601	221(266)
1	-5373.77	-5.2175	-4.4917	0.725	-
S-2	-5452.39	-5.1601	-4.4275	0.732	-

R-3	-5452.40	-5.1870	-4.4577	0.729	-
4	-5320.14	-6.1367	-2.6163	3.520	352(282)
S-5	-5398.77	-6.0357	-2.5219	3.513	352(284)
R-6	-5398.76	-6.0842	-2.5448	3.539	350(283)
7	-5112.71	-6.4175	-1.8073	4.610	268(266)
S-8	-5191.34	-6.2556	-1.7181	4.537	273(269)
R-9	-5191.34	-6.3761	-1.7565	4.619	268(269)

Optimized geometry of **L^1-L^3** gives the required orientation of alcoholic -OH groups essential for the formation of metallomacrocyclic xanthate complexes **1**, S-**2**, R-**3**, **4**, S-**5**, R-**6**, **7**, S-**8,** R-**9**. In the binuclear M^{II} xanthate metallomacrocyclic complexes **1**, S-**2**, R-**3**, **4**, S-**5**, R-**6**, **7**, S-**8** and R-**9**, optimized geometries clearly suggest that each xanthate ligands bridge two metal centres via chelating xanthate moieties, resulting in the formation of binuclear metallomacrocyclic architectures. The optimized structures (Figure 3) clearly revealed distorted square planar coordination geometry around Ni^{II} and Cu^{II} nucleus in respective binuclear metallamacrocyclic complexes (**1**, S-**2**, R-**3**, **4**, S-**5**, R-**6**) whereas distorted tetrahedral coordination geometry around each Zn^{II} centres in their corresponding metallamacrocyclic complexes (**7**, S-**8** and R-**9**).

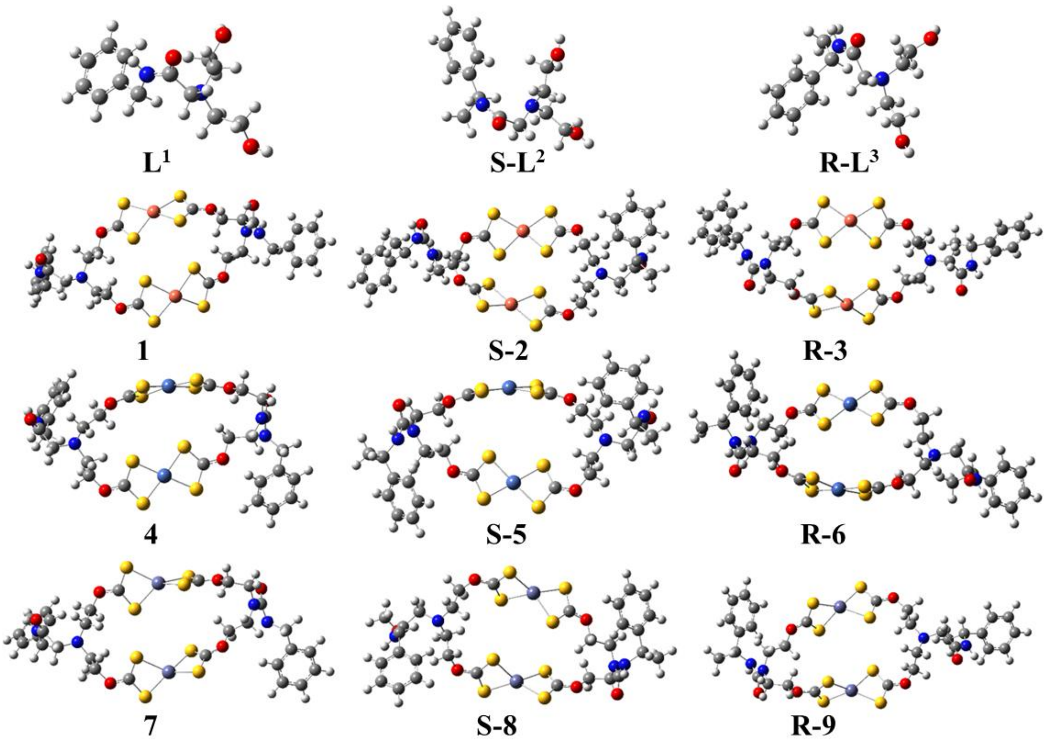

Figure 3. An optimized geometry for the minimum energy conformation of all diol ligand precursors (L^1, S-L^2 and R-L^3) and their xanthate complexes with Cu^{II}, Ni^{II}, Zn^{II} (**1**, S-**2**, R-**3**, **4**, S-**5**, R-**6**, **7**, S-**8** and R-**9)** at B3LYP/LanL2DZ level.

Table 7. Selected geometrical parameters (average values) obtained from the optimized geometry of all ligand (L^1, L^2 and L^3) and their xanthate complexes with Cu^{II}, Ni^{II}, Zn^{II} (**1**, S-**2**, R-**3**, **4**, S-**5**, R-**6**, **7**, S-**8** and R-**9**).

Entry	**Selected Bond**	**Bond lengths [Å]**	**Selected Bonds**	**Bond angles [°]**
L1	O-C	1.423	O-C-C	106.41
S-L2	O-C	1.423	O-C-C	106.26
R-L3	O-C	1.423	O-C-C	106.67
1	O-C	1.452	O-C-S	120.8
	O-C (CS_2)	1.323	S-C-S (Chelate)	118.37
	C-S	1.713	S-Cu-S(Chelate)	74.91
	S-Cu	2.419	S-Cu-S	106.44
	Cu-Cu	6.244	S-Cu-S (Trans)	163.51
S-2	O-C	1.453	O-C-S	120.8
	O-C (CS_2)	1.322	S-C-S (Chelate)	118.32
	C-S	1.713	S-Cu-S(Chelate)	74.88
	S-Cu	2.419	S-Cu-S	106.42
	Cu-Cu	6.271	S-Cu-S (Trans)	163.11
R-3	O-C	1.453	O-C-S	120.83
	O-C (CS_2)	1.322	S-C-S (Chelate)	118.32
	C-S	1.713	S-Cu-S(Chelate)	74.88
	S-Cu	2.42	S-Cu-S	106.18
	Cu-Cu	6.262	S-Cu-S (Trans)	162.92
4	O-C	1.453	O-C-S	121.83
	O-C (CS_2)	1.32	S-C-S (Chelate)	115.8
	C-S	1.717	S-Ni-S(Chelate)	78.53
	S-Ni	2.289	S-Ni-S	101.38
	Ni-Ni	5.855	S-Ni-S (Trans)	175.42
S-5	O-C	1.451	O-C-S	122.13
	O-C (CS_2)	1.319	S-C-S (Chelate)	115.72
	C-S	1.711	S-Ni-S(Chelate)	78.55
	S-Ni	2.289	S-Ni-S	101.23
	Ni-Ni	6.05	S-Ni-S (Trans)	174.44
R-6	O-C	1.451	O-C-S	122.12
	O-C (CS_2)	1.319	S-C-S (Chelate)	115.73
	C-S	1.711	S-Ni-S(Chelate)	78.54
	S-Ni	2.288	S-Ni-S	101.23
	Ni-Ni	6.036	S-Ni-S (Trans)	174.4
7	O-C	1.449	O-C-S	118.74
	O-C (CS_2)	1.323	S-C-S (Chelate)	122.52
	C-S	1.723	S-Zn-S(Chelate)	75.89
	S-Zn	2.457	S-Zn-S	129.2
	Zn-Zn	6.253	S-Zn-S (Trans)	130.47
S-8	O-C	1.448	O-C-S	118.76
	O-C (CS_2)	1.322	S-C-S (Chelate)	122.47
	C-S	1.724	S-Zn-S(Chelate)	75.92
	S-Zn	2.456	S-Zn-S	129.26

	Zn-Zn	6.239	S-Zn-S (Trans)	127.02
S-9	O-C	1.449	O-C-S	118.77
	O-C (CS_2)	1.322	S-C-S (Chelate)	122.46
	C-S	1.723	S-Zn-S(Chelate)	75.91
	S-Zn	2.456	S-Zn-S	129.6
	Zn-Zn	6.244	S-Zn-S (Trans)	126.69

The theoretical values of structural parameters (average) for M^{II} xanthate metallomacrocyclic complexes are summarized in Table 7. The experimental data of two closely related Ni^{II} xanthate metallomacrocyclic complexes[xx-yy] have been retrieved from the literature to carry out the comparison of structural parameters with similar parameters obtained theoretically for our Ni^{II} xanthate metallomacrocyclic complexes **4**, S-**5**, R-**6**. A careful comparison revealed that in case of Ni^{II} metallamacrocyclic complexes **4**, S-**5** and R-**6**, the average bond distances such as C-S (1.71 Å), Ni-S (2.29 Å) and average bond angles trans S—M—S (175˚) and Chelate S-Ni-S (79˚) are very close to the similar parameters of those obtained from X-ray study (Table 7).

Table 8. Selected geometrical parameters (average values) obtained from X-ray structures [19]

Entry	Selected Bond	Bond lengths [Å]	Selected Bonds	Bond angles [˚]
		dinuclear nickel(II) xanthate macrocycle[14]		
	O-C	1.459	O-C-S	123.24
	O-C (CS_2)	1.304	S-C-S (Chelate)	113.5
	C-S	1.689	S-Ni-S(Chelate)	79.56
	S-Ni	2.208	S-Ni-S	99.44
	Ni-Ni	4.286	S-Ni-S (Trans)	177.62
		$[Ni^{II}_2$-μ^2-bis-$\{(\kappa^2 S,S$-$S_2COCH_2CH_2)_2N(Ts)\}]$[21]		
	O-C	1.455	O-C-S	123.39
	O-C (CS_2)	1.307	S-C-S (Chelate)	113.2
	C-S	1.697	S-Ni-S(Chelate)	79.36
	S-Ni	2.22	S-Ni-S (outer)	100.94
	Ni-Ni	4.57	S-Ni-S (Trans)	177.78

8.3.4.2 Molecular electrostatic potential

The mapping of molecular electrostatic potential (MESP) of ligand (L^1, L^2 and L^3) and complexes **1**, S-**2**, R-**3**, **4**, S-**5**, R-**6**, **7**, S-**8** and R-**9** clearly determines the projection of polar amide subunits towards the open-air. Further, it reveals the existence of negative potential at the amidic oxygen and positive potential at the amidic proton. (Figure 4) This, apparently suggest the ability these molecules to form H-bonding interactions and to facilitate interactions with biomolecules, required for better biological activity through effective cellular membrane transportation.[22]

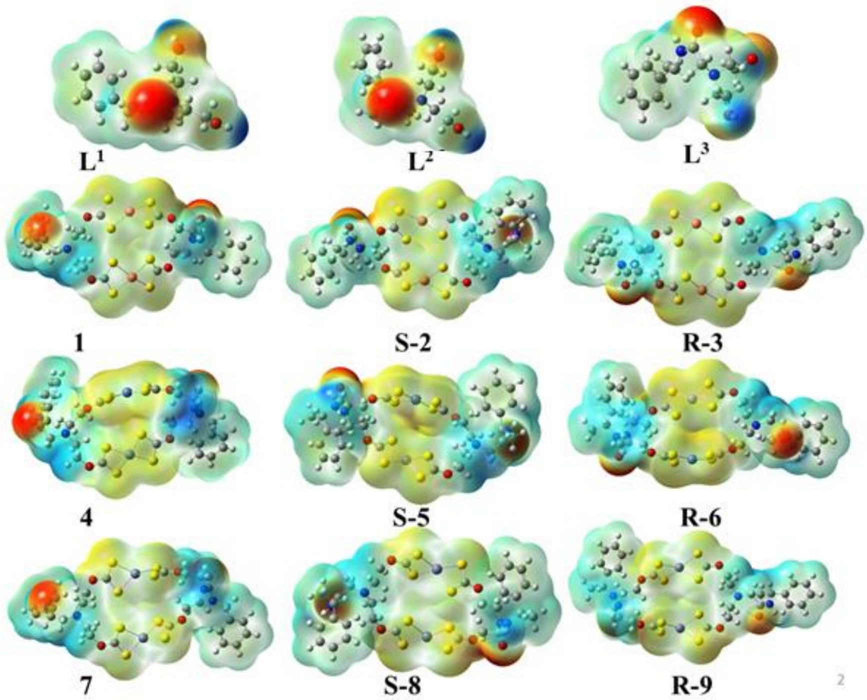

Figure 4. Representations of electron density from total SCF density (Isovalue= 0.0004; mapped with ESP)

Moreover, an examination of frontier molecular orbitals becomes important for the prediction of the potential reactivity and photo-physical properties of the molecules. The energy of optimization and HOMO-LUMO band gaps for all of these complexes are tabulated in Table 6. A comparison of the frontier molecular orbitals derived from DFT calculation at the B3LYP/LANL2DZ level for ligand L^1-L^3 and their xanthate complexes **1**, S-**2**, R-**3**, **4**, S-**5**, R-**6**, **7**, S-**8** and R-**9** are provided in Figure 5. It may be noted that for L^1-L^3, the HOMO is localized over alkyl chain and LUMO is delocalized over aromatic ring. However, in case of the M^{II}xanthate complexes HOMO as well as LUMO (Figure 5) is predominantly localized over coordinated xanthate functionality. The increasing order of HOMO-LUMO band gaps of these complexes follows the trend Cu < Ni < Zn. Interestingly, HOMO-LUMO energy band gaps obtained for binuclear metallomacrocyclic Cu^{II}-xanthate complexes 1, S-**2** and and R-**3** falls in the range of 0.729-0.732 eV, suggestive of the semiconducting nature of these compounds.[23]

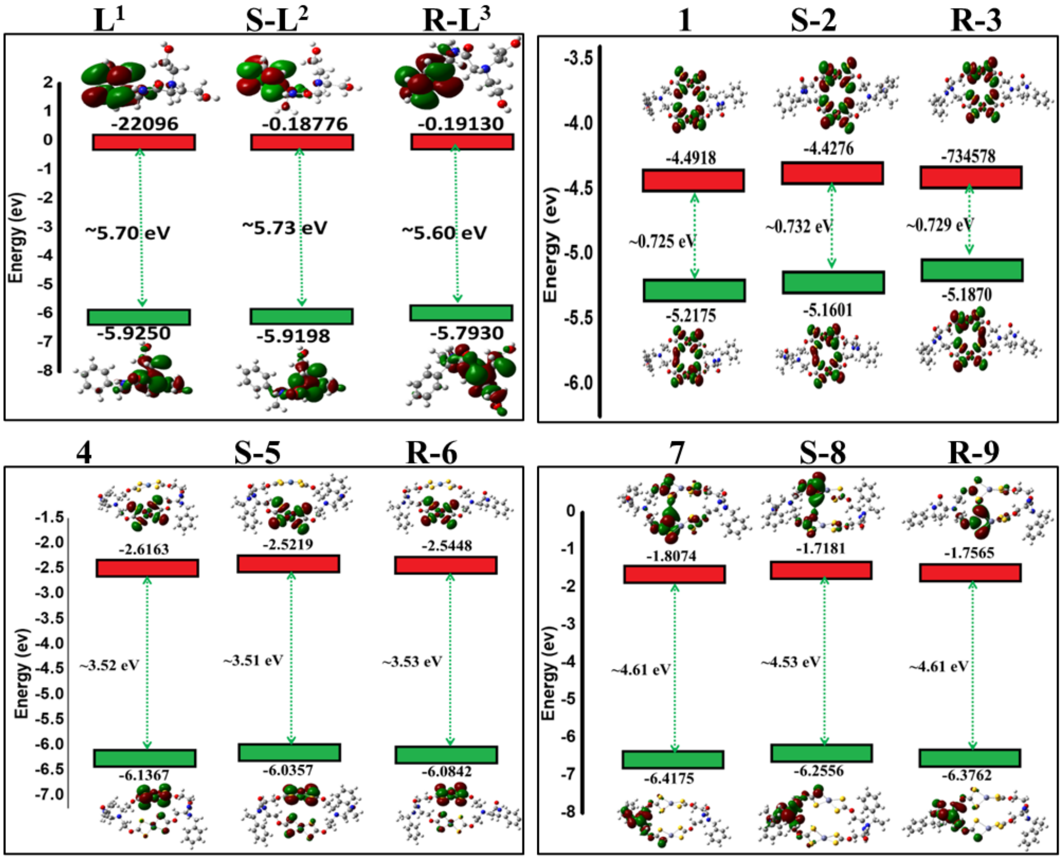

Figure 5. Comparison of the frontier molecular orbitals derived from DFT calculation at the B3LYP/LANL2DZ level for ligand (L^1, L^2 and L^3) and complexes Cu^{II}, Ni^{II} and Zn^{II} complexes (**1**, S-**2**, R-**3**, **4**, S-**5**, R-**6**, **7**, S-**8** and R-**9)**

8.4 Conclusions

This chapter describes the synthesis and characterization of new chiral/achiral diol ligand precursors viz. N-benzyl-2-(bis(2-hydroxyethyl)amino)acetamide (**L^1**), (S)-2-(bis(2-hydroxyethyl)amino)-N-(1-phenylethyl)acetamide (**L^2**), (R)-2-(bis(2-hydroxyethyl)amino)-N-(1-phenylethyl)acetamide (**L^3**) and ensuing binuclear metallamacrocyclic complexes of type [M^{II}_2-μ^2-bis-{(κ^2S,S-$S_2COCH_2CH_2)_2N(CH_2CONH(CH(G)Ph))$}] {G=H, M= Cu^{II} **1**, G=CH_3, M= Cu^{II} S-**2**, G=CH_3, M= Cu^{II} R-**3**, G=H, M= Ni^{II} **4**, G=CH_3, M= Ni^{II} S-**5**, G=CH_3, M= Ni^{II} R-**6**, G=H, M= Zn^{II} **7**, G=CH_3, M= Zn^{II} S-**8** and G=CH_3, M= Zn^{II} R-**9}** holding pendent amido groups in the ligand framework. Compounds were suitably characterized by microanalysis, HRMS and other relevant spectroscopic techniques viz. FT- IR, UV-visible, ^{1}H and ^{13}C NMR. Molecules of L^3 are stabilized by a number of weak intermolecular interactions in the solid state as revealed by single crystal XRD. Evidently, molecules of L^3 forms a fascinating S-shaped 1D molecular architecture by involving intermolecular hydrogen bonding interactions.

The absorption spectral study along with magnetic susceptibility measurements determined distorted square-planar geometry around Cu^{II} and Ni^{II} centres and distorted tetrahedral geometry around Zn^{II} centres in their respective complexes. A DFT level calculations have been performed on all the diol ligand precursors (**L^1-L^3**) and M^{II}-xanthate complexes (**1, S-2, R-3, 4, S-5, R-6, 7, S-8, R-9**) at B3LYP/LanL2DZ level. Notably, Cu^{II}-xanthate complexes **1**, **S-2**, **R-3** gave HOMO-LUMO energy band gaps in the range of 0.725-0.732 eV and determine their semiconducting nature. The mapping of molecular electrostatic potential (MESP) of all the complexes revealed that positive charges are mainly accumulated amidic NH whereas negative charges are localized at amidic CO. This shows the potentials of these molecules to facilitate an effective H-bonding interactions in the biological systems.

8.5 Reference

[1] (a) S. J. Dalgarno, S. A. Tucker, D. B. Bassil, J. L. Atwood, *Science*, **2005**, 309, 2037; (b) V. Percec, A. E. Dulcey, V. S. K. Balagurusamy, Y. Miura, J. Smidrkal, M. Peterca, S. Nummelin, U. Edlund, S. D. Hudson, P. A. Heiney, H. Duan, S. N. Magonov, S. A. Vinogradov, *Nature*, **2004**, 430, 764; (c) G. R. Desiraju, *J. Am. Chem. Soc.*, **2013**, 135, 9952. (d) J. M. Lehn, *Science*, **1985**, 227, 849; (e) G. M. Whitesides, B. Grzybowski, *Science*, **2002**, 295, 2418.

[2] (a) M. T. Kirchner, D. Bläser, R. Boese, *Chem. Eur. J.*, **2010**, 16, 2131; (b) D. Braga, F. Grepioni, G. R. Desiraju, *Chem. Rev.*, **1998**, 98, 1375.

[3] (a) J. C. Noveron, M. S. Lah, R. E. D. Sesto, A. M. Arif, J. S. Miller, P. J. Stang, *J. Am. Chem. Soc.*, **2002**, 124, 6613; (b) A. G. L. Olive, K. Parkan, C. Givelet, J. Michl, *J. Am. Chem. Soc.*, **2011**, 133, 20108; (c) M. Yamagami, T. Sawada, M. Fujita, *J. Am. Chem. Soc.*, **2018**, 140, 8644; (d) V. C. -H. Wong, C. Po, S. Y.-L. Leung, A. K.-W. Chan, S. Yang, B. Zhu, X. Cui, V. W. -W. Yam, *J. Am. Chem. Soc.*, **2018**, 140, 657; (e) M. S. Collins, N. M. Phan, L. N. Zakharov, D. W. Johnson, *Inorg. Chem.*, **2018**, 57, 3486; (f) P. N. W. Baxter, J. M. Lehn, G. Baum,

D. Fenske, *Chem. Eur. J.*, **1999**, 5, 102; (g) V. W.-W. Yam, V. K.-M. Au, S. Y. -L. Leung, *Chem. Rev.*, **2015**, 115, 7589.

[4] (a) J. Cookson, E. A. L. Evans, J. P. Maher, C. J. Serpell, R. L. Paul, A. R. Cowley, M. G. B. Drew, P. D. Beer, *Inorg. Chim. Acta*., **2010**, 363, 1195; (b) E. S. Juárez, J. C. Huerta, I. F. H. Ahuactzi, R. R. Martínez, H. Tlahuext, H. M. Rojas, H. Höpfl, *Inorg. Chem.,* **2008**, 47, 9804.

[5] (a) E. G. Percástegui, L. N. Zakharov, J. G. A. Rodríguez, M. E. Carnes and D. W. Johnson, *Cryst. Growth Des.*, **2014**, 14, 2087; (b) V. K. Singh, R. Kadu, H. Roy, P. Raghavaiah and S. M. Mobin, *Dalton Trans.*, **2016**, 45, 1443.

[6] (a) V. Pillai, S. K. Patel, L. Buch, V. K. Singh, *Appl Organometal Chem.*, **2018**, 32, 4559; (b) R. Kadu, H. Roy, V. K. Singh, *Appl. Organomet. Chem*., **2015**, 29, 746; (c) V. Pillai, L. Buch, A. Desai, V. K. Singh, *ChemistrySelect*, **2017**, 2, 11581.

[7] R. J. Puddephatt, *Chem. Soc. Rev*., **2008**, 37, 2012.

[8] R. R. Martínez, P. G. García, M. L. Cardoso, H. Höpfl, H. Tlahuext, *Dalton Trans*., **2008**, 6624.

[9] P. D. Beer, N. G. Berry, A. R. Cowley, E. J. Hayes, E. C. Oates, W. W. H. Wong, *Chem. Commun.*, **2003**, 2408.

[10] (a) J. A. Sinsel, R. L. Bardun, C. H. Peterson, *J. Food Sci.*, **1986**, 51, 424; (b) F. F. Horne, C. Valley, Calif, US Patent, US3797646A.

[11] (a) E. M. Driggers, S. P. Hale, J. Lee, N. K. Terrett, *Nat. Rev. Drug Discov*., **2008**, 7, 608; (b) J. Mallinson and I. Collins, *Future Med Chem*., **2012**, 4, 1409; (c) A. Mann in The Practice of Medicinal Chemistry, (Ed: C. G. Wermuth), Academic Press, London, UK, **2008**, 1.

[12] (a) V. K. Singh, R. Kadu, H. Roy, P. Raghavaiah, S. M. Mobin, *Dalton Trans*., **2016**, 45, 1443; (b) V. Pillai, R. Kadu, L. Buch, V. K. Singh, *ChemistrySelect*, **2017**, 2, 4382.

[13] (a) A. Alama, B. Tasso, F. Novelli, F. Sparatore, *Drug Discov. Today*, **2009**, 14, 500; (b) A. Kamal, B. A. Kumar, M. Arifuddin, S. G. Dastidar, *Bioorg. Med. Chem*., **2003**, 11, 5135; (c) Y. Singh, M. Palombo, P. J. Sinko, *Curr. Med. Chem*., **2008**, 15, 1802; (d) G. Faraglia, D. Fregona, S. Sitran, L. Giovagnini, C. Marzano, F. Baccichetti, U. Casellato, R. Graziani, *J. Inorg. Biochem.*, **2001**, 83, 31.

[14] P. D. Beer, A. R. Cowley, J. C. Jeffery, R. L. Paul, W.W.H. Wong, *Polyhedron*, **2003**, 2795.

[15] Watt and McCormick, *Spectrochimica Acta*, **1965**, 21, 753.

[16] (a) D. R. V. Staveren, N. Metzler-Nolte, *Chem. Rev*., **2004**, 104, 5931; (b) S. K. Verma, V. K. Singh, *J. Organomet. Chem*., **2015**, 791, 214; (c) S. K. Verma, V. K. Singh, *Polyhedron*, **2014**, 76, 1.

[17] V. K Singh, V. Pillai, S. K. Patel, L. Buch, *Chemistry Select,* **2019**, 4, 8689.

[18] Leininger, B. Olenyuk, P. J. Stang, *Chem. Rev*., **2000**, 100, 853.

[19] M. J. Frisch, G. W. Trucks, H. B. Schlegel, G. E. Scuseria, M. A. Robb, J. R. Cheeseman, G. Scalmani, V. Barone, G. A. Petersson, H. Nakatsuji, X. Li, M. Caricato, A. V. Marenich, J. Bloino, B. G. Janesko, R. Gomperts, B. Mennucci, H. P. Hratchian, J. V. Ortiz, A. F. Izmaylov, J. L. Sonnenberg, D. Williams-Young, F. Ding, F. Lipparini, F. Egidi, J. Goings, B. Peng, A. Petrone, T. Henderson, D. Ranasinghe, V. G. Zakrzewski, J. Gao, N. Rega, G. Zheng, W. Liang, M. Hada, M. Ehara, K. Toyota, R. Fukuda, J. Hasegawa, M. Ishida, T. Nakajima, Y. Honda, O. Kitao, H. Nakai, T. Vreven, K. Throssell, J. A. Montgomery, Jr, J. E. Peralta, F. Ogliaro, M. J. Bearpark, J. J. Heyd, E. N. Brothers, K. N. Kudin, V. N. Staroverov, T. A. Keith, R. Kobayashi, J. Normand, K. Raghavachari, A. P. Rendell, J. C. Burant, S. S. Iyengar, J. Tomasi, M. Cossi, J. M. Millam, M. Klene, C. Adamo, R. Cammi, J. W. Ochterski, R. L. Martin, K. Morokuma, O. Farkas, J. B. Foresman, D. J. Fox, Gaussian, Inc. Wallingford CT, **2016**.

[20] (a) X. Yu, N. Wang, H. He, L. Wang, *SpectrochimActa A*, **2014**, 122, 283; (b) D. Ghosh, K. Sen, A. K. Das, *Struct Chem*., **2012**, 23, 227; (c) M. Dolores Palacios, M. C. Puerta, P. Valerga, A. Lledos, E. Veilly, *Inorg. Chem.*, **2007**, 46, 6958.

[21] R. Kadu, K. Kolte, C. Savani, S. S. Zade, A. A. Isab, A. K. Singh, V. K. Singh, *New J. Chem.*, **2022**, under revision.

[22] (a) S. R. Gadre, P. K. Bhadane, *Resonance*, **1999**, 4, 11; (b) F. A. Bulat, A. T. -Labbé, T. Brinck, J. S. Murray, P. Politzer, *J Mol Model*, **2010**, 16, 1679; (b) P. Politzer, P. R. Laurence, K. Jayasuriya, Environ. *Health Perspect*., **1985**, 61, 191.

[23] R. Kadu, V. K. Singh, S. K. Verma, P. Raghavaiah, M. M. Shaikh, *J Mol. Struct*., **2013**, 1033, 298.

8.6 Annexures

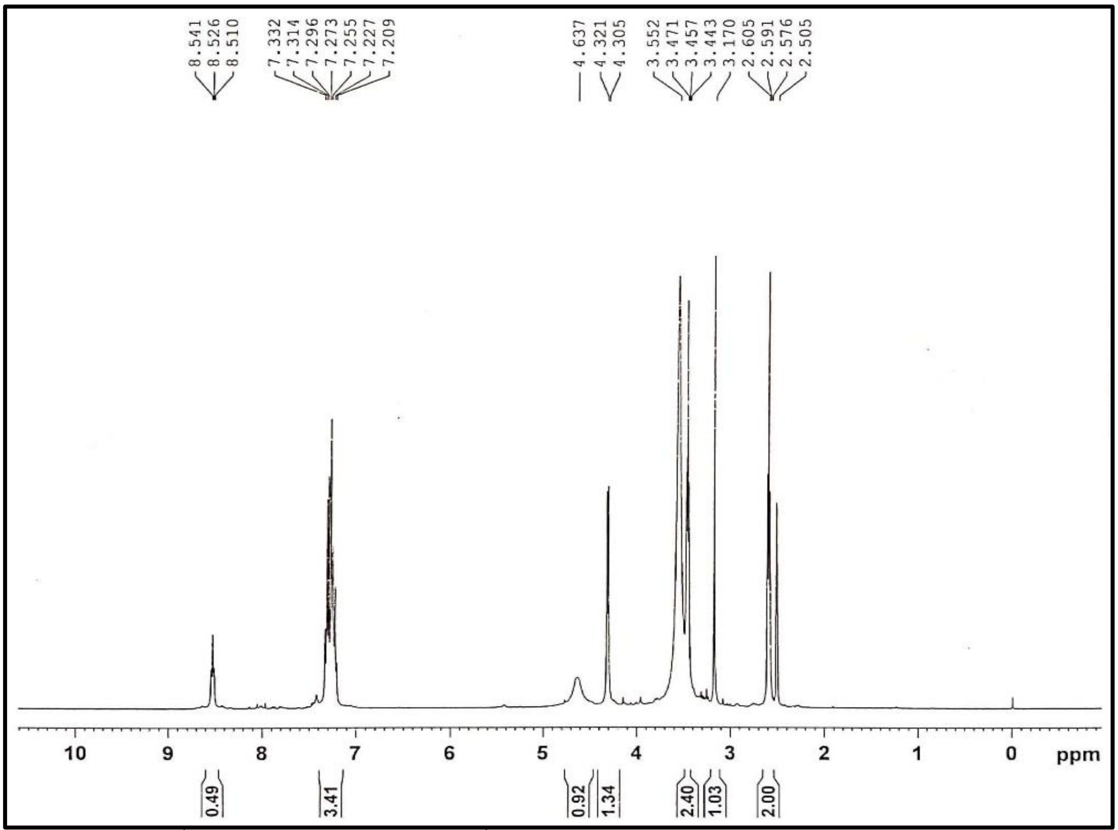

Annexure 1. [1]H NMR spectrum of L[1].

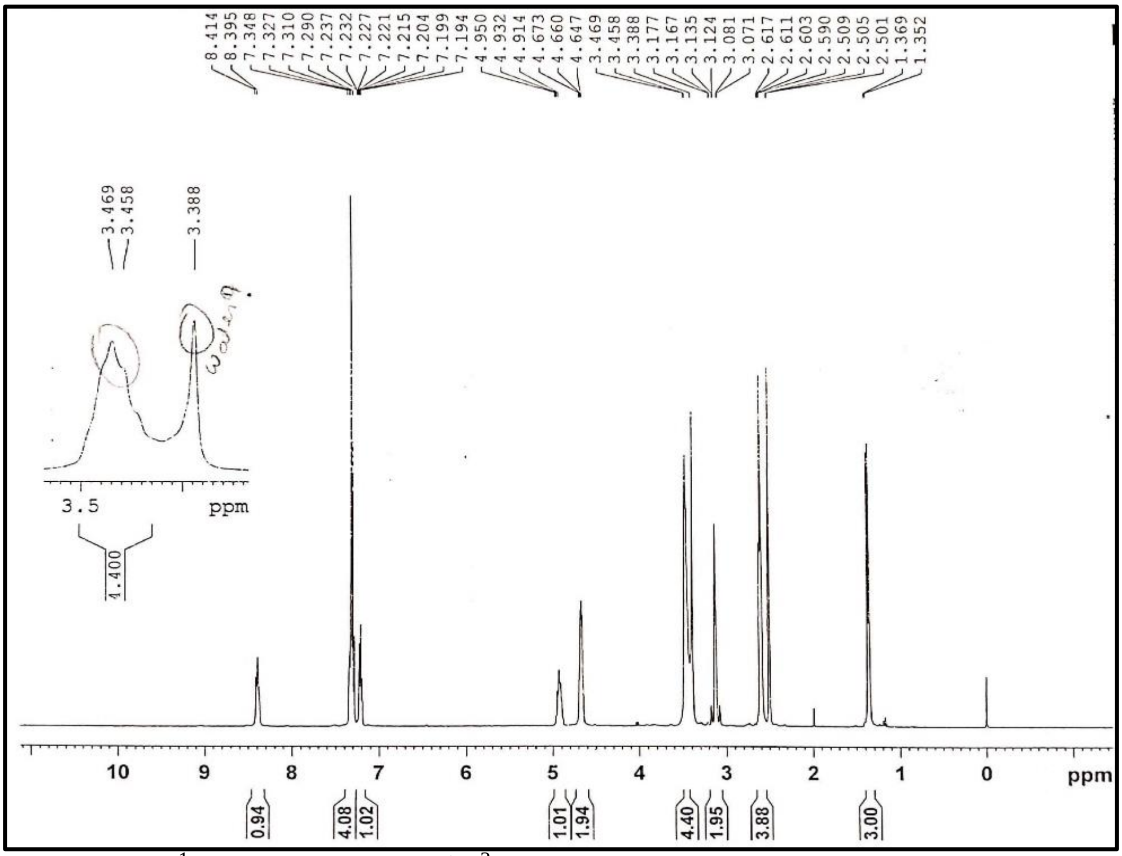

Annexure 2. [1]H NMR spectrum of L[2].

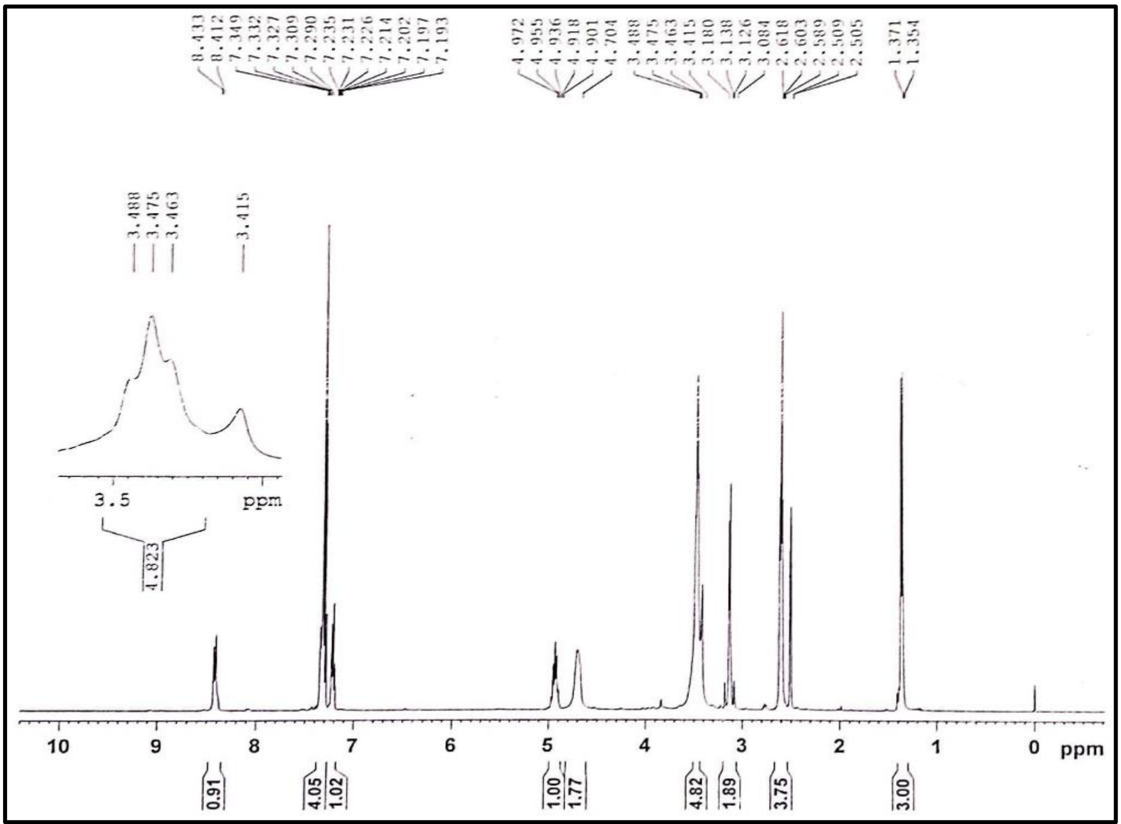

Annexure 3. ^{1}H NMR spectrum of L^3.

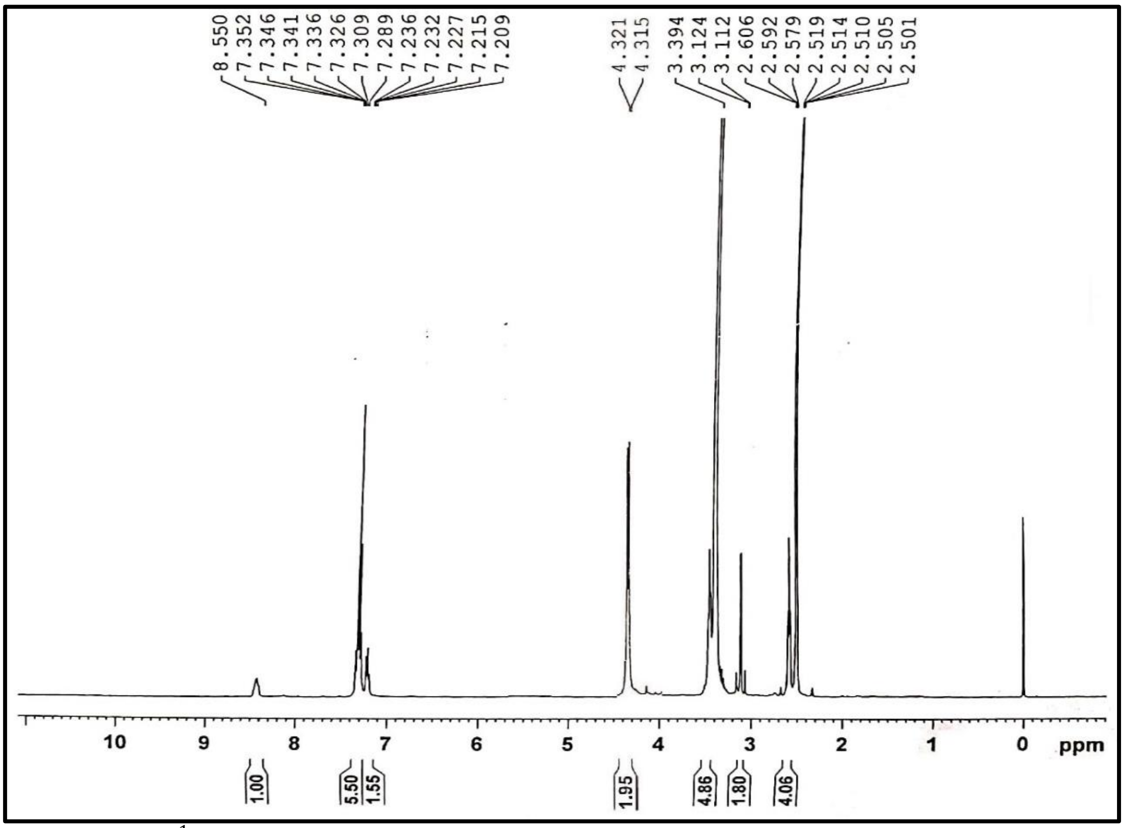

Annexure 4. ^{1}H NMR spectrum of 7.

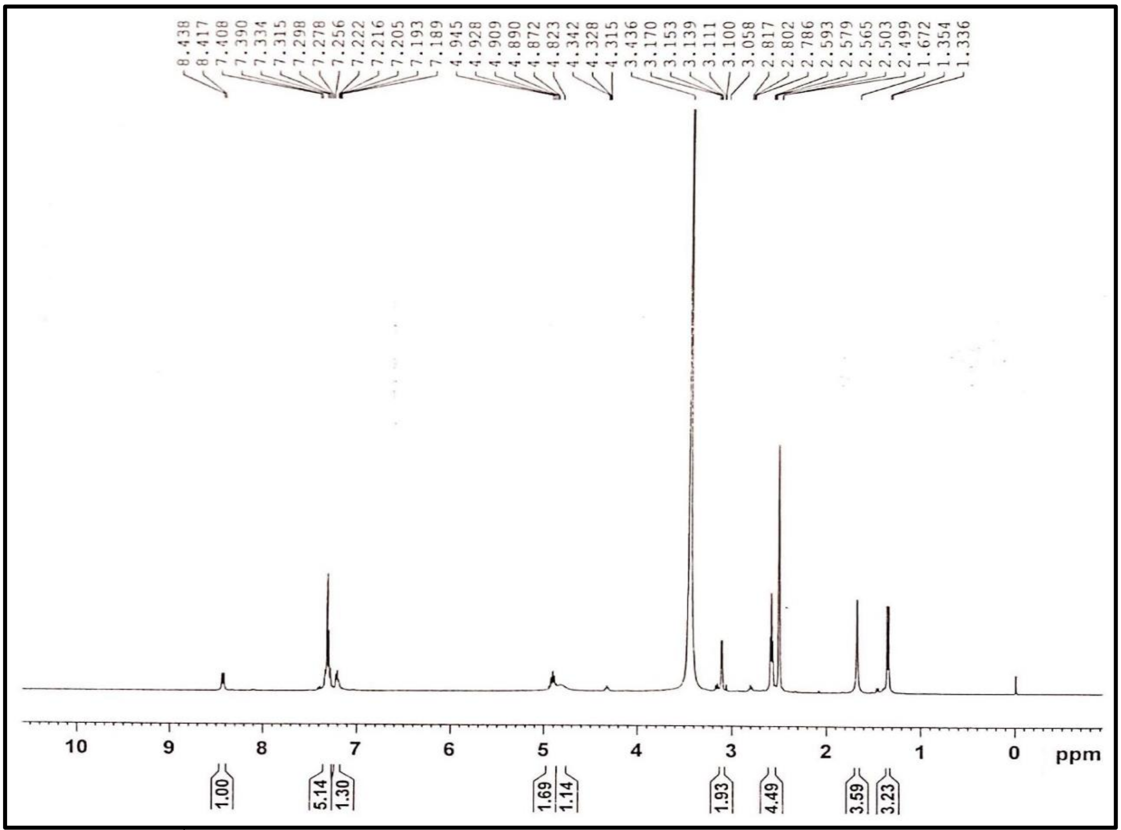

Annexure 5. ^{1}H NMR spectrum of S-8.

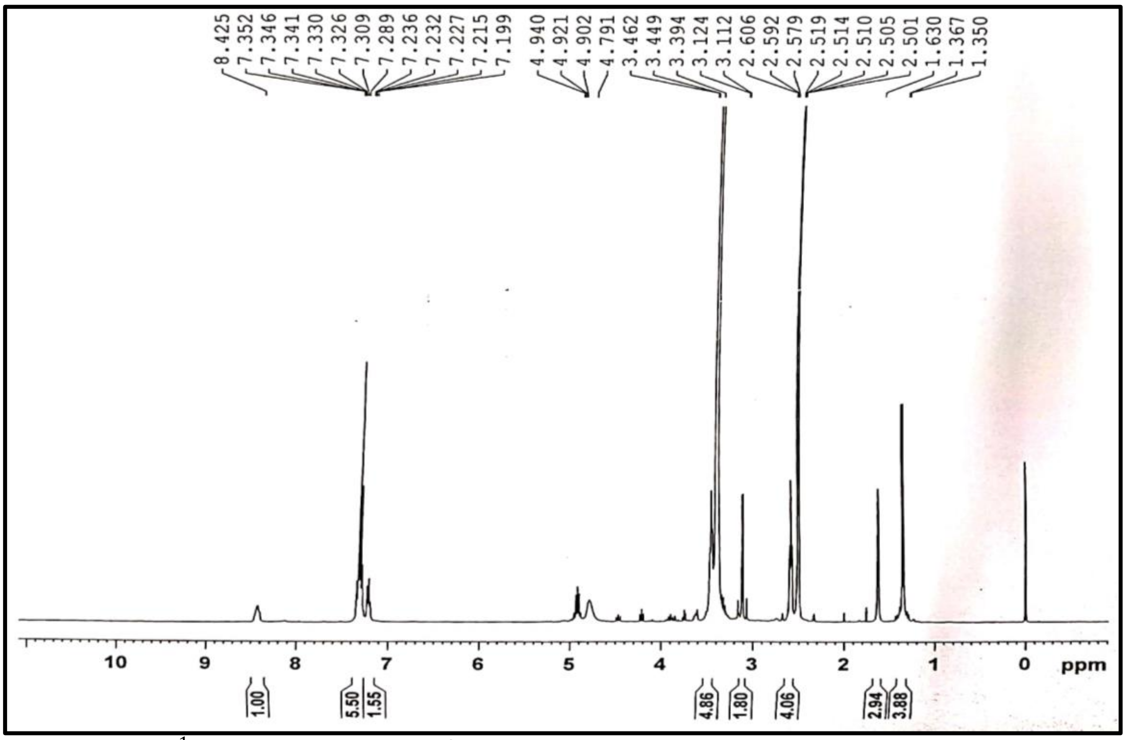

Annexure 6. ^{1}H NMR spectrum of R-9.

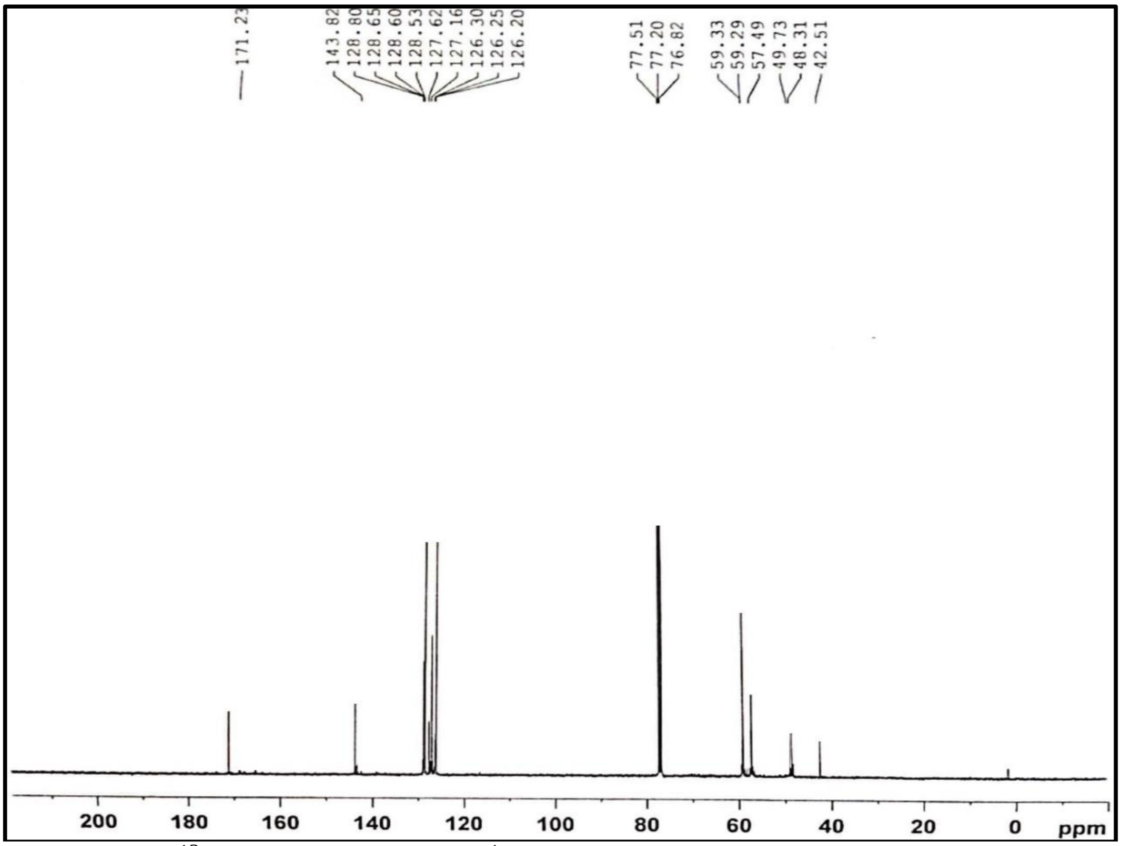

Annexure 7. ^{13}C NMR spectrum of L^1.

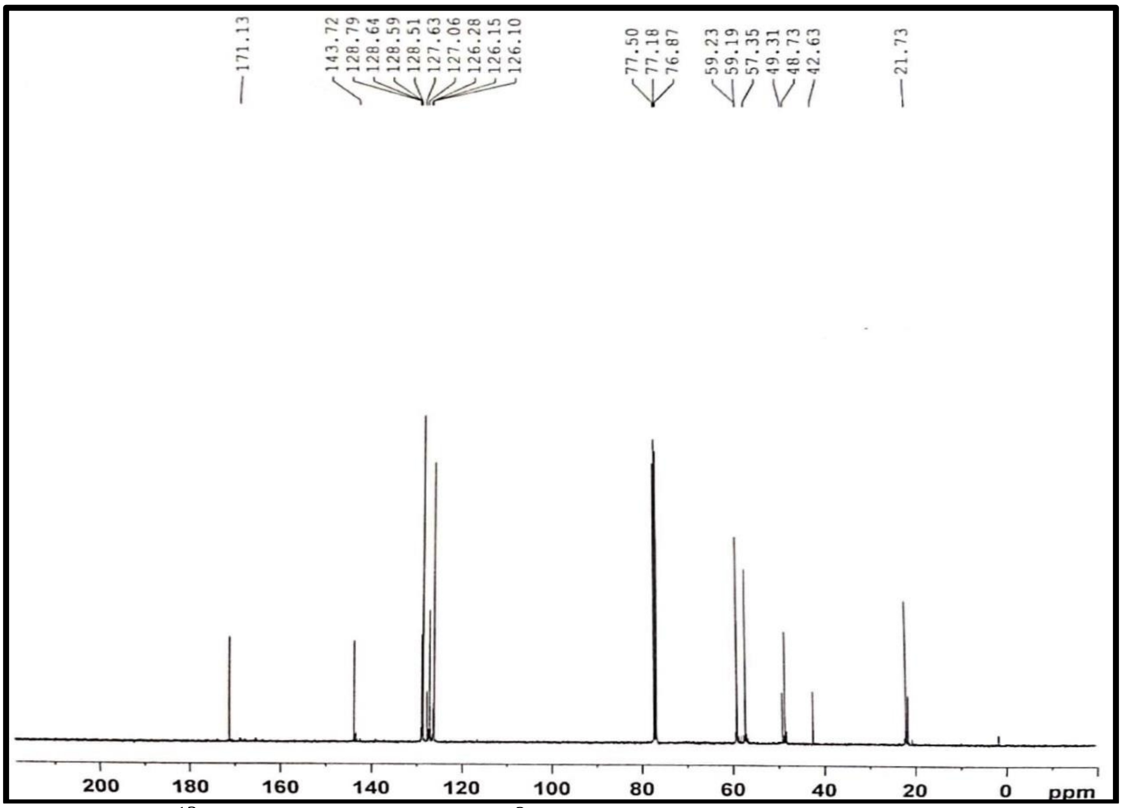

Annexure 8. ^{13}C NMR spectrum of S-L^2.

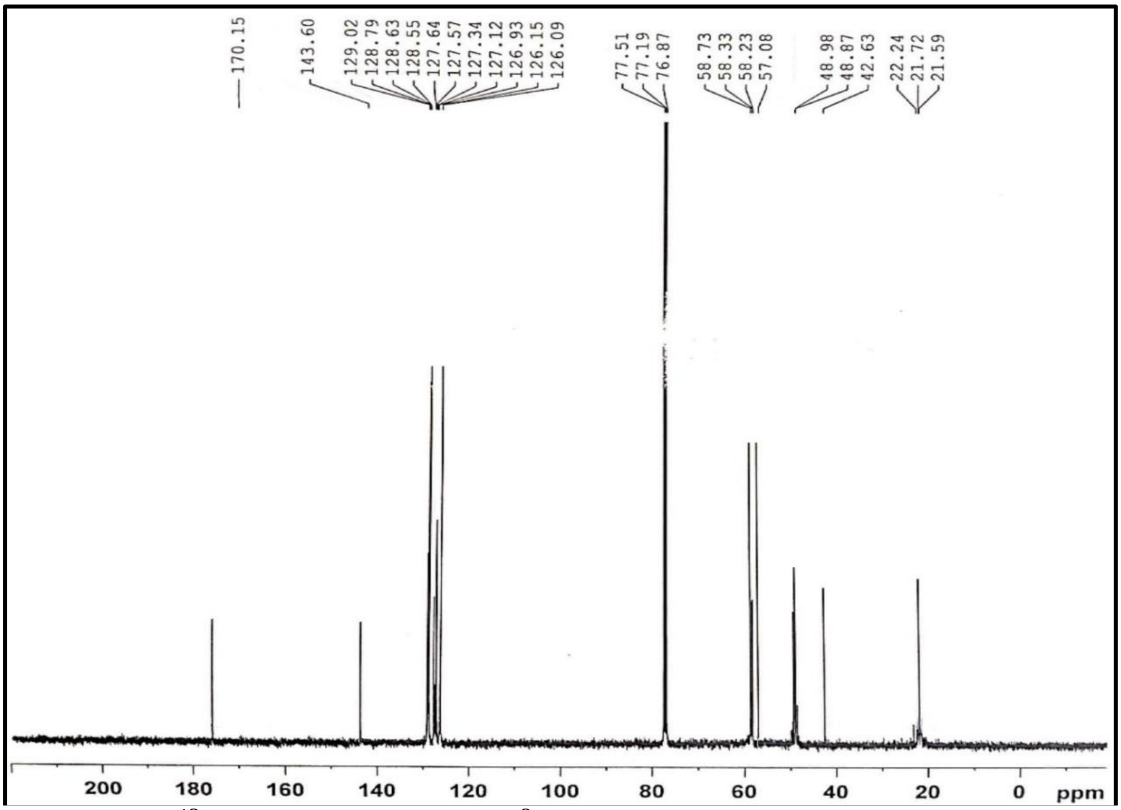

Annexure 9. ^{13}C NMR spectrum of R-L^3.

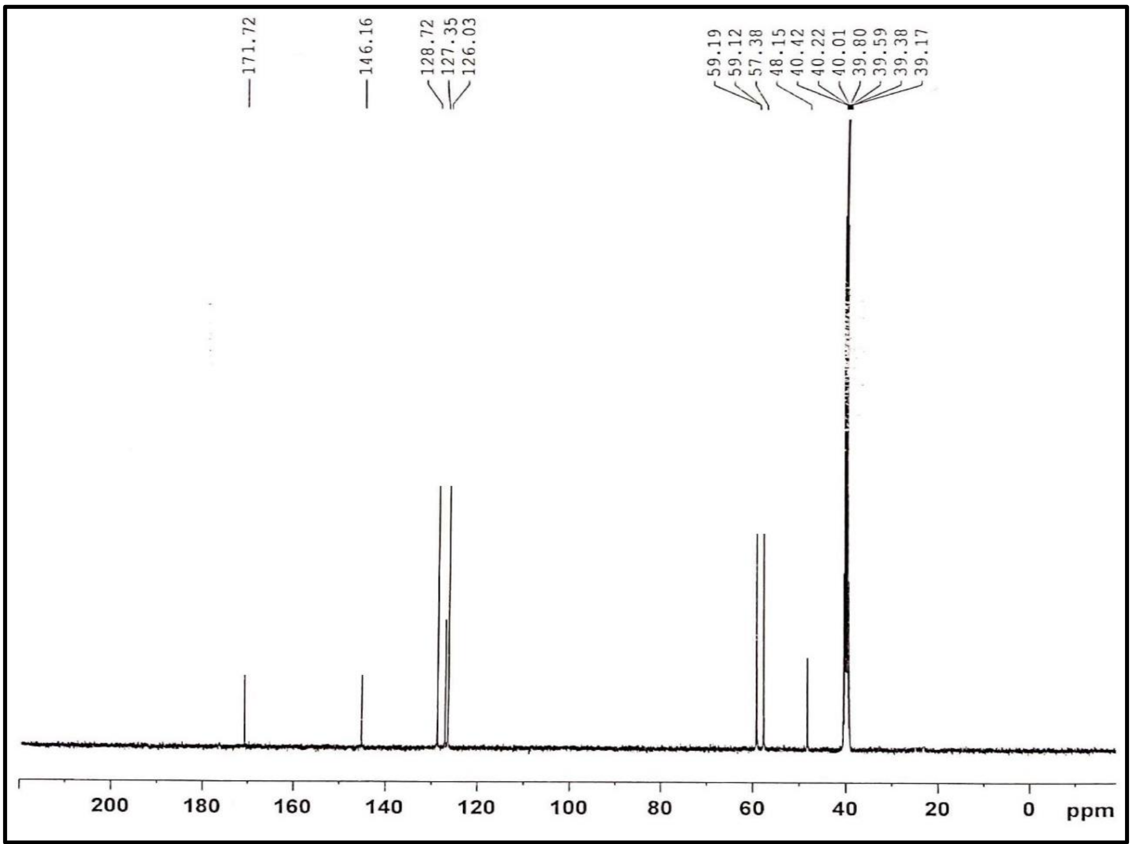

Annexure 10. ^{13}C NMR spectrum of 7.

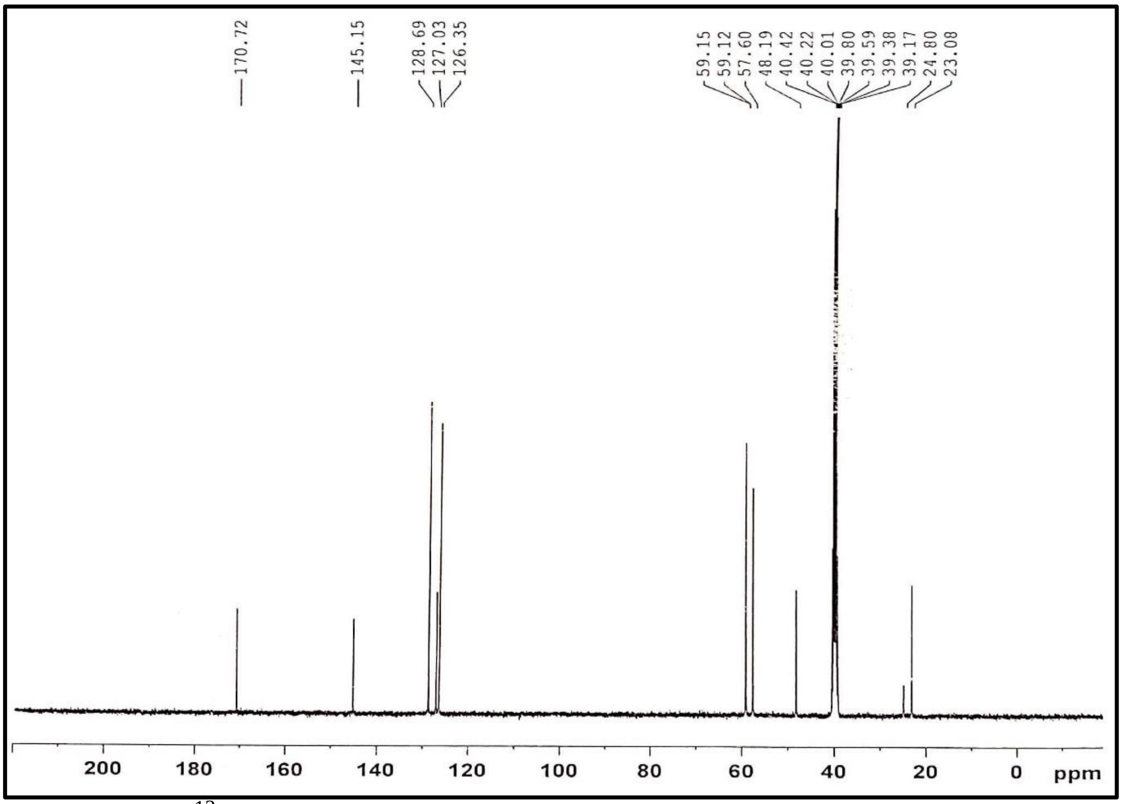

Annexure 11. ^{13}C NMR spectrum of S-8.

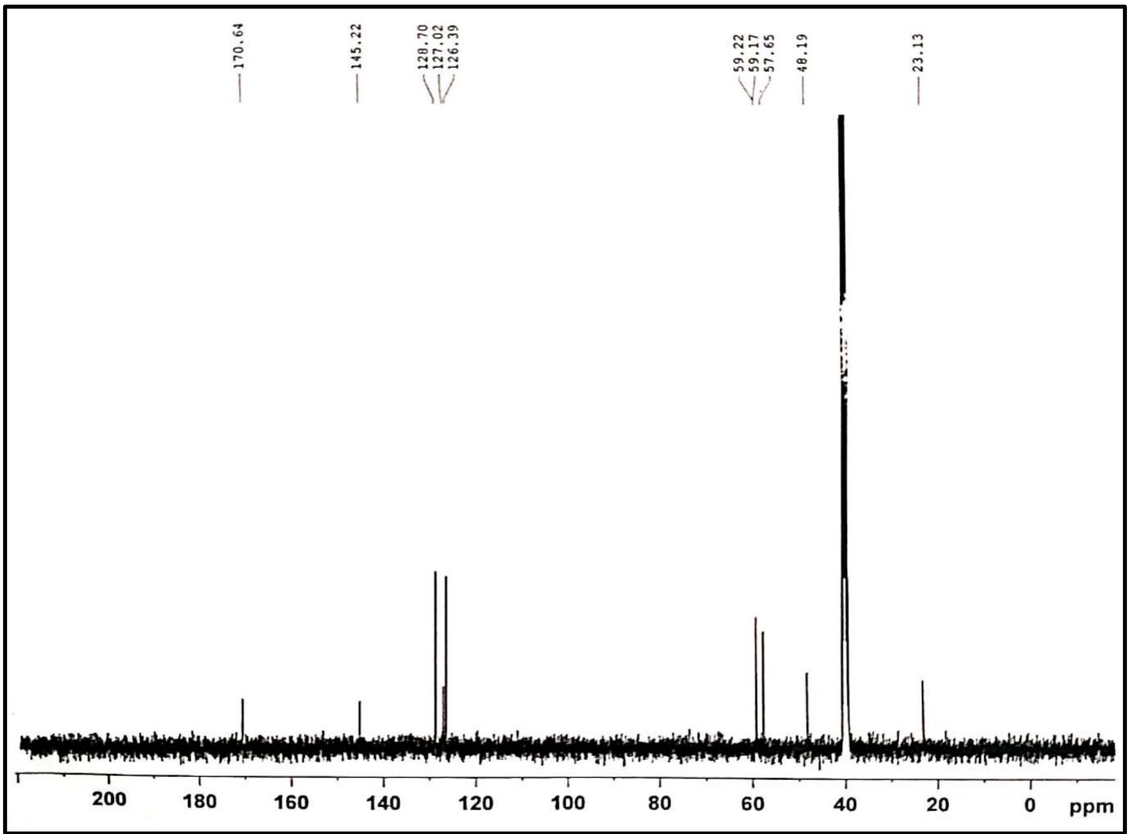

Annexure 12. ^{13}C NMR spectrum of R-9.

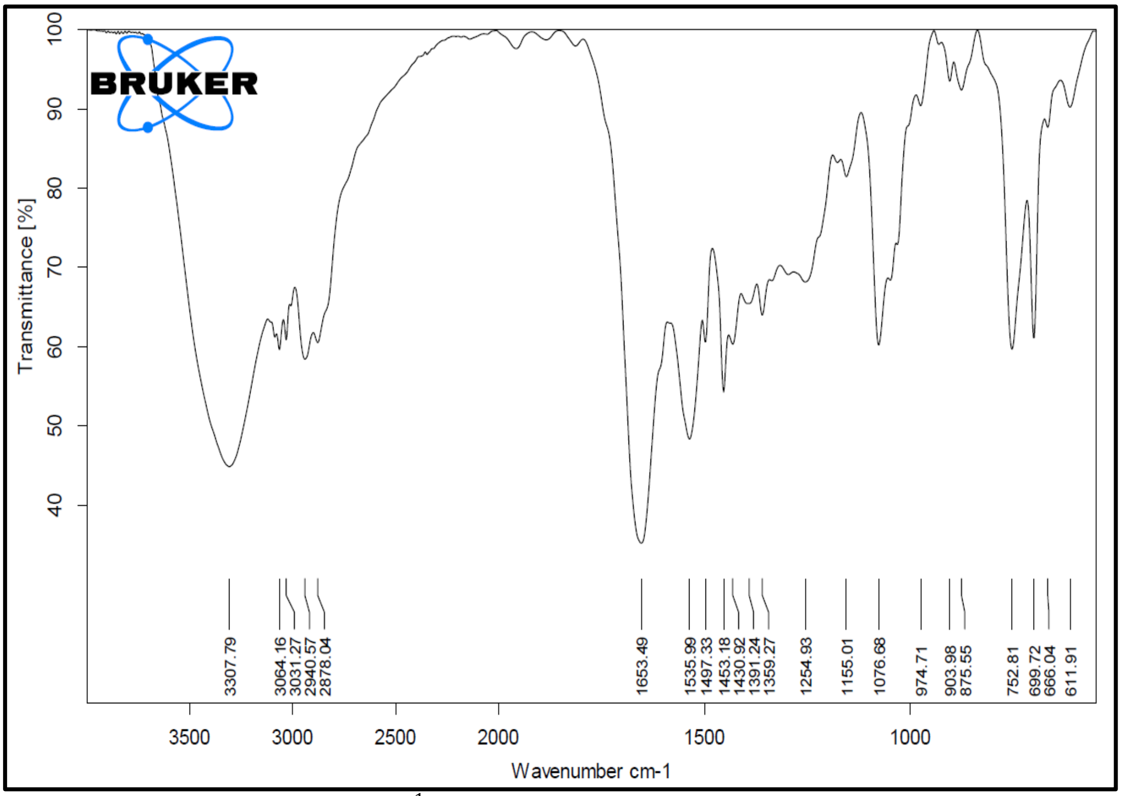

Annexure 13. IR spectrum of L^1.

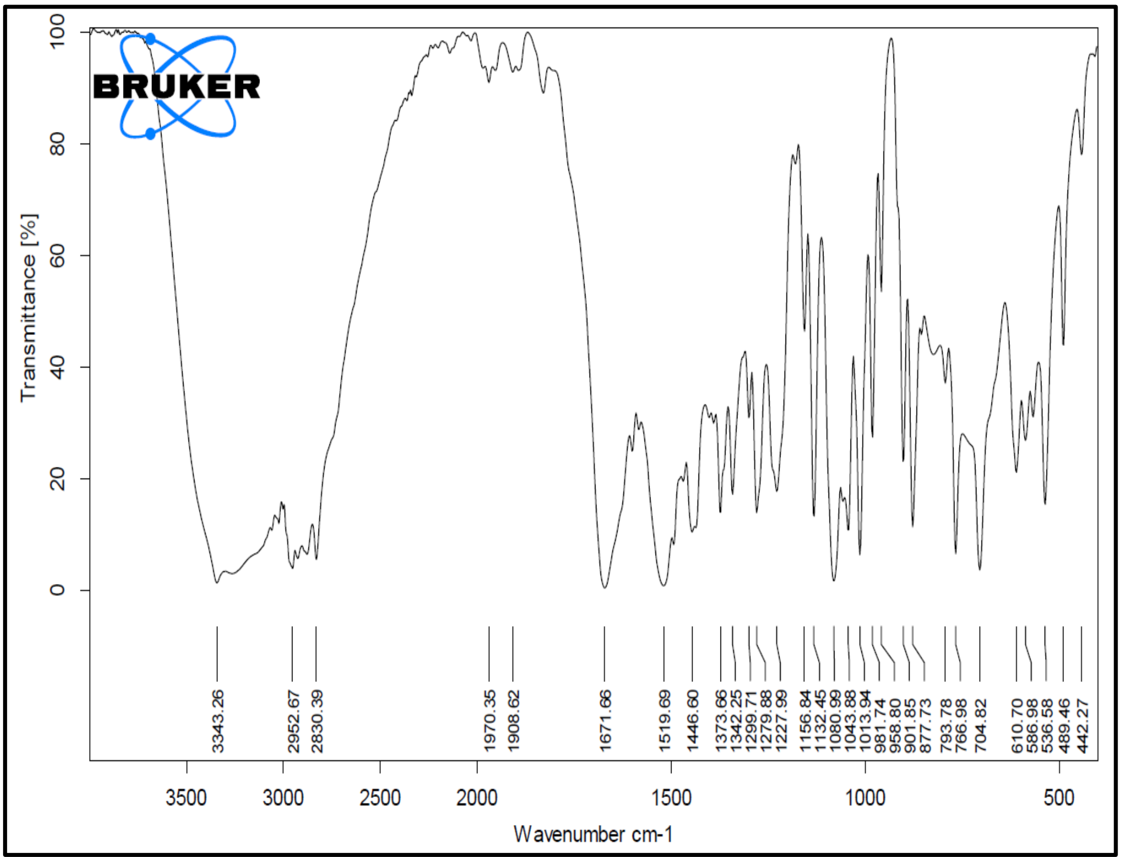

Annexure 14. IR spectrum of L^2.

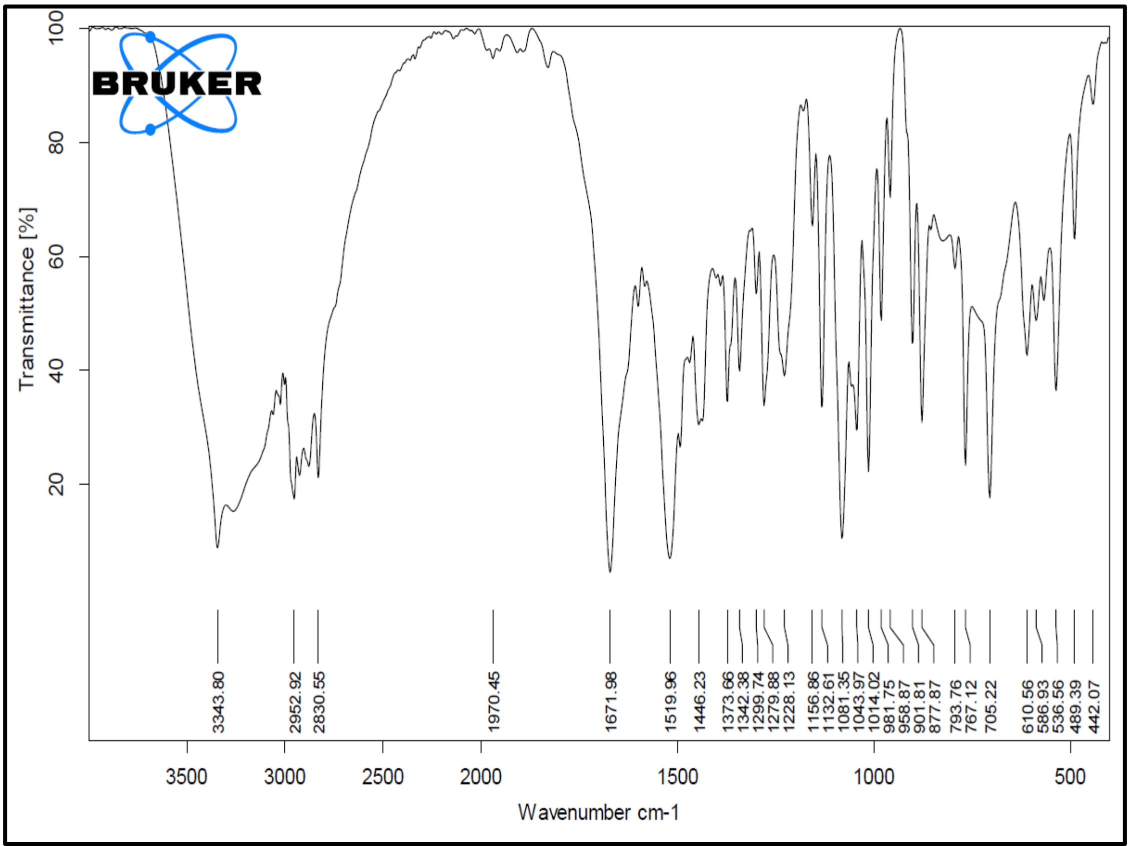

Annexure 15. IR spectrum of L^3.

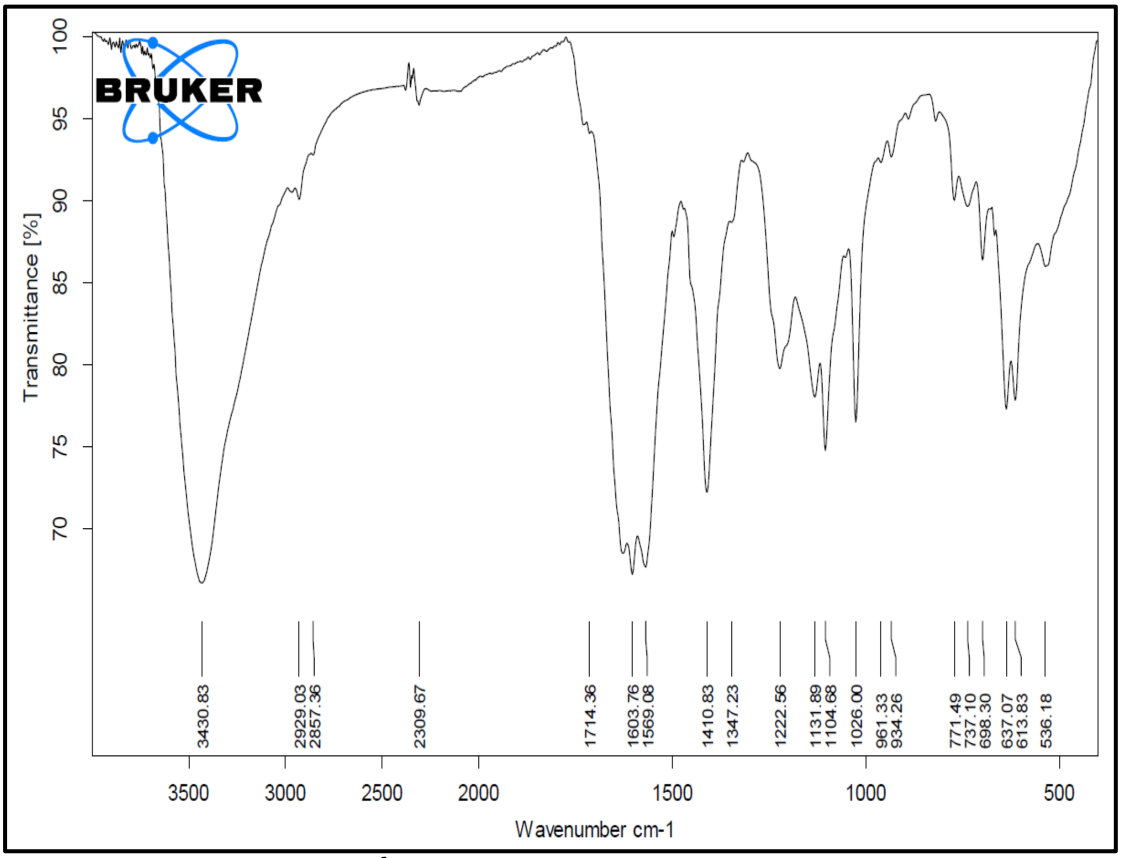

Annexure 16. IR spectrum of 1.

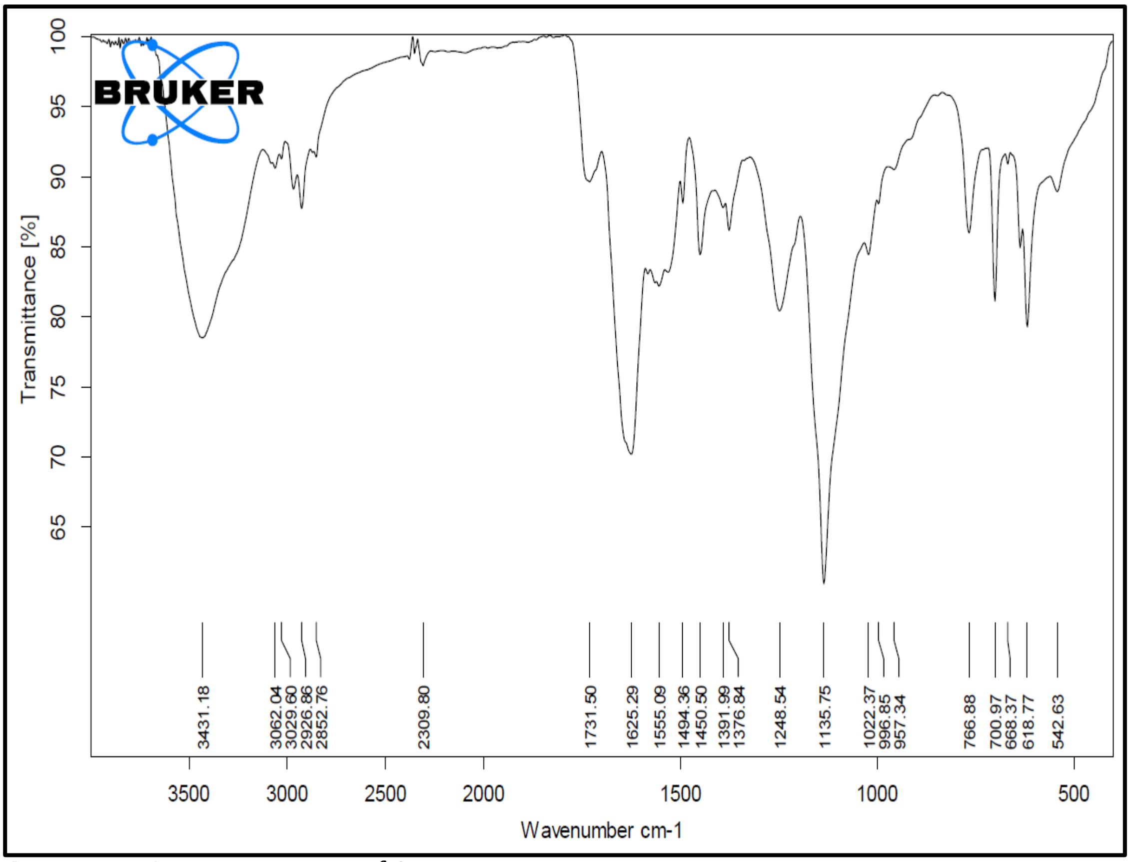

Annexure 17. IR spectrum of 2.

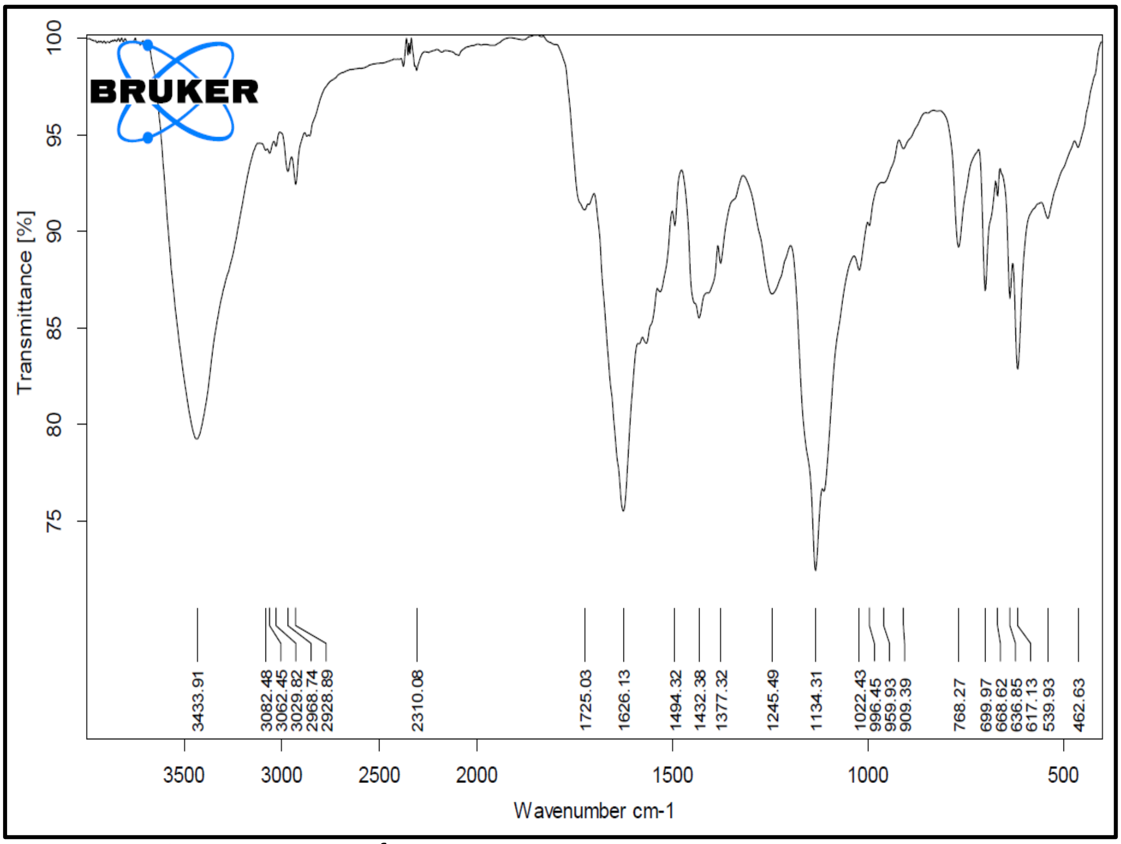

Annexure 18. IR spectrum of 3.

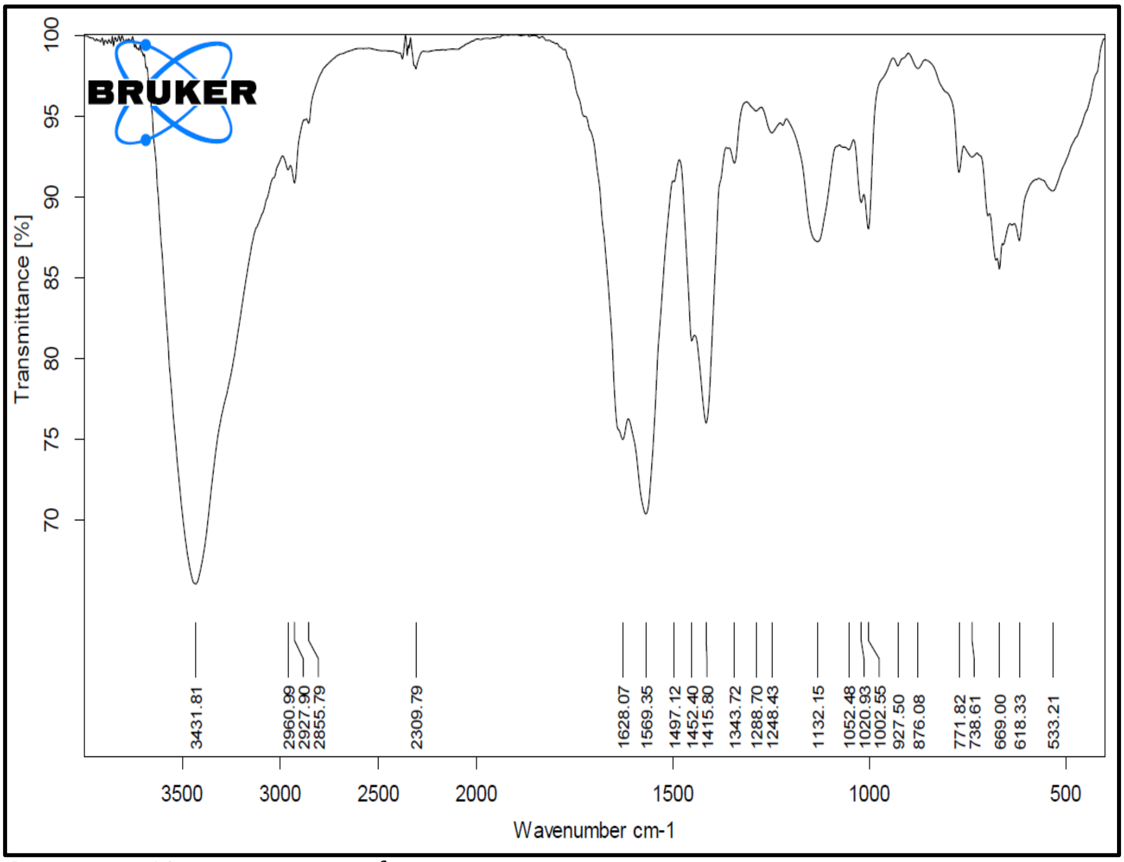

Annexure 19. IR spectrum of 4.

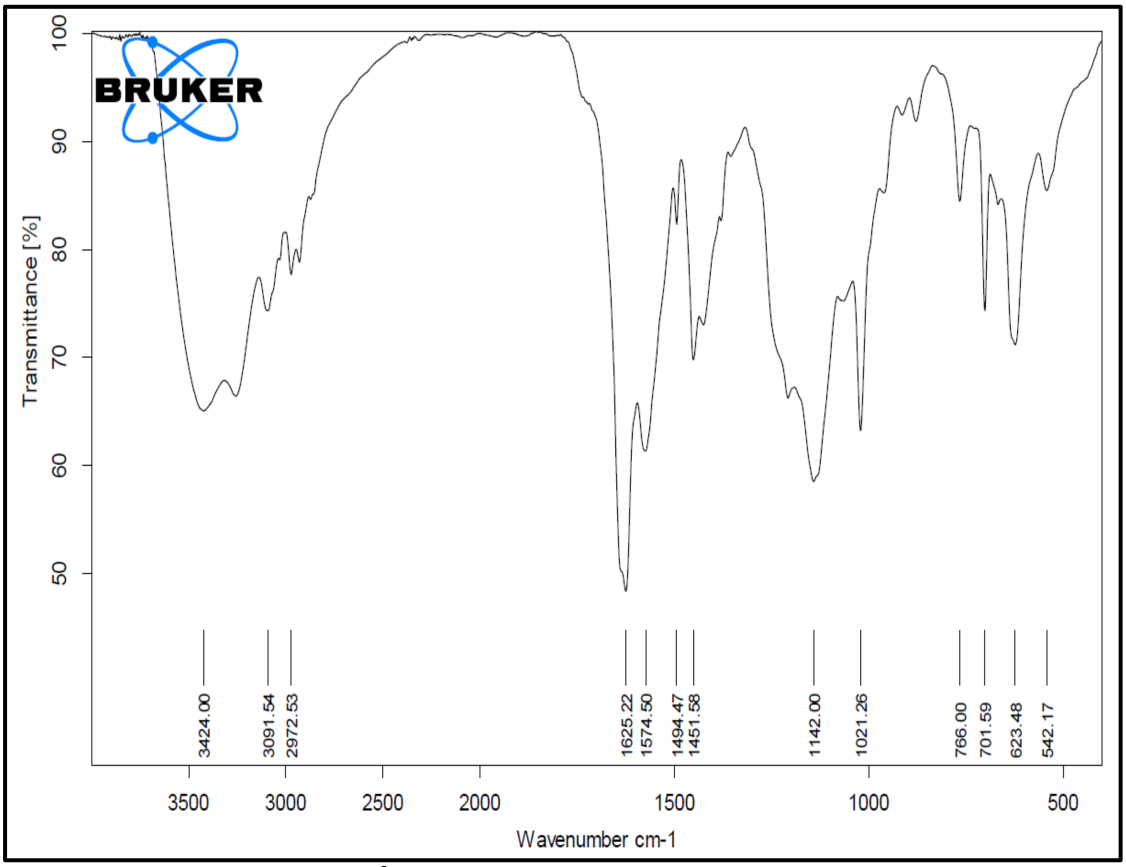

Annexure 20. IR spectrum of 5.

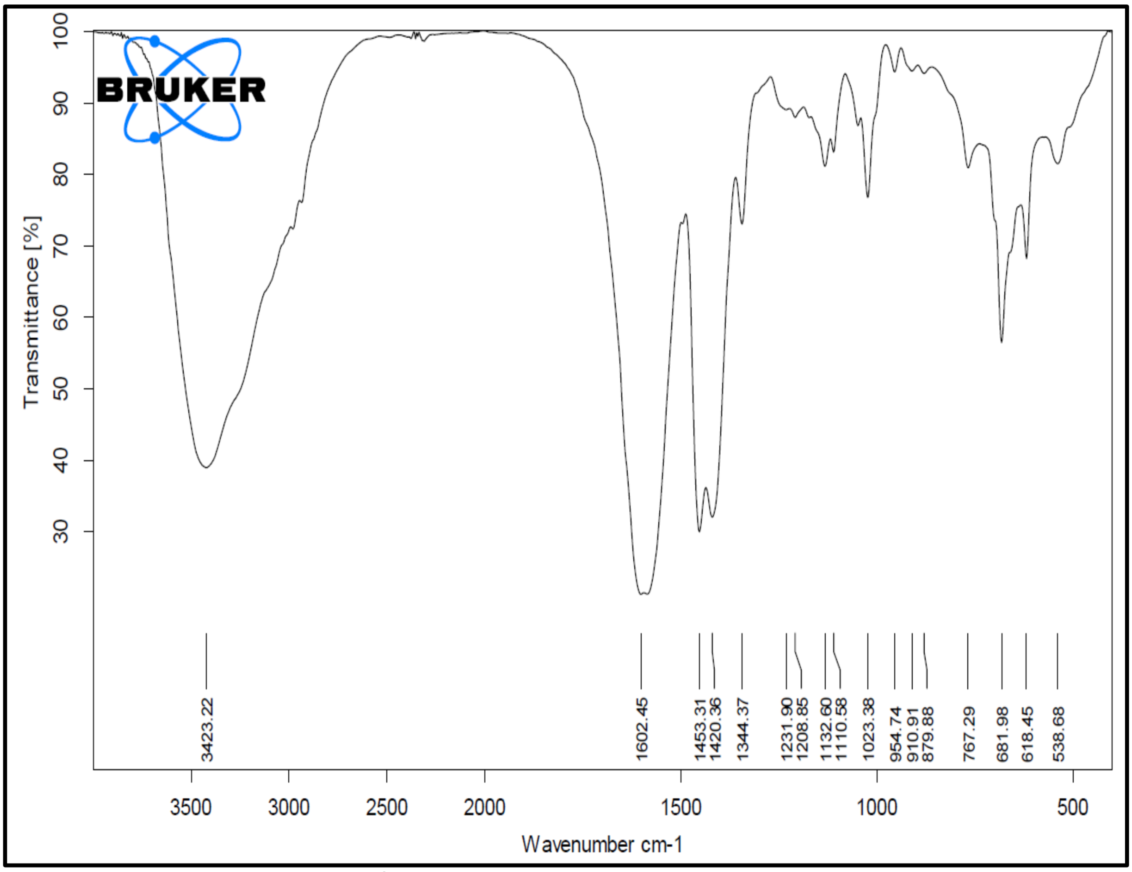

Annexure 21. IR spectrum of 6.

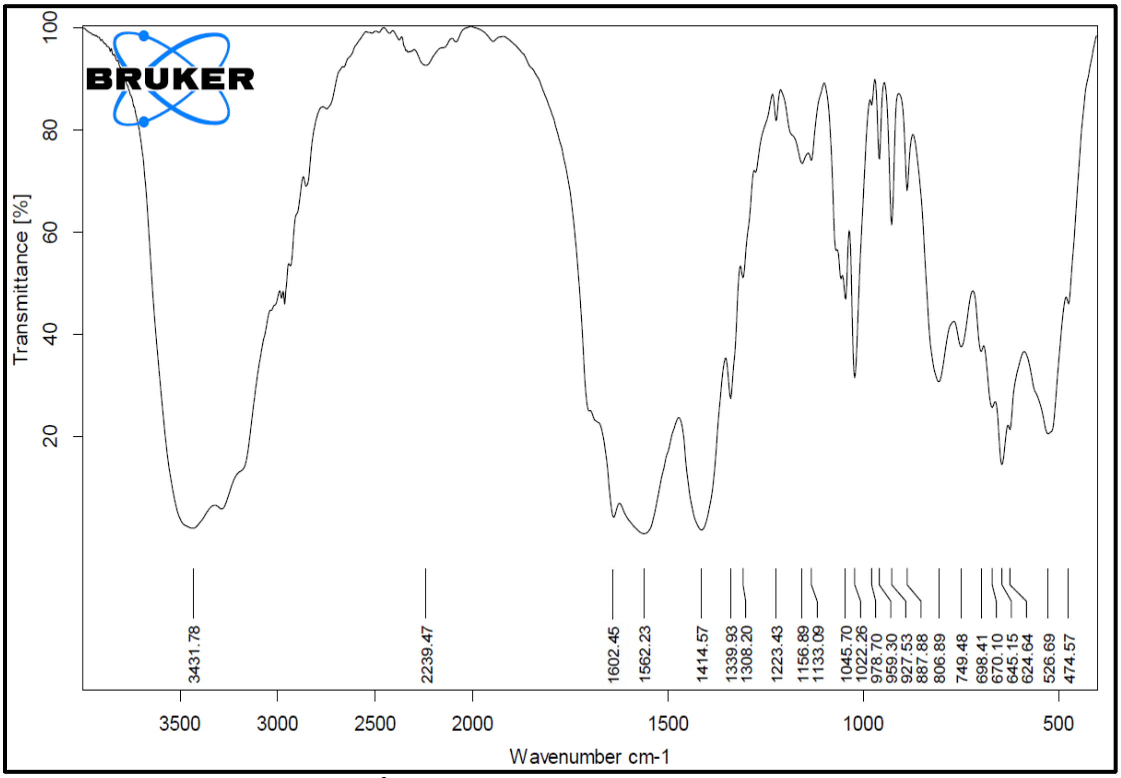

Annexure 22. IR spectrum of 7.

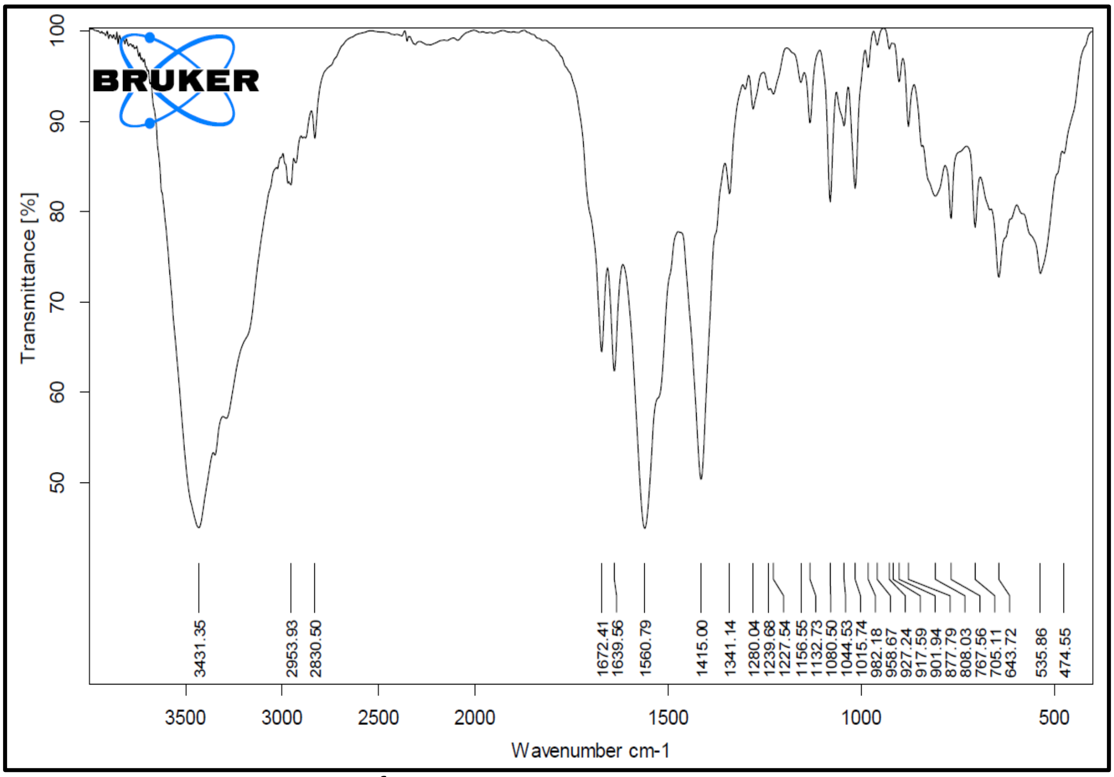

Annexure 23. IR spectrum of 8.

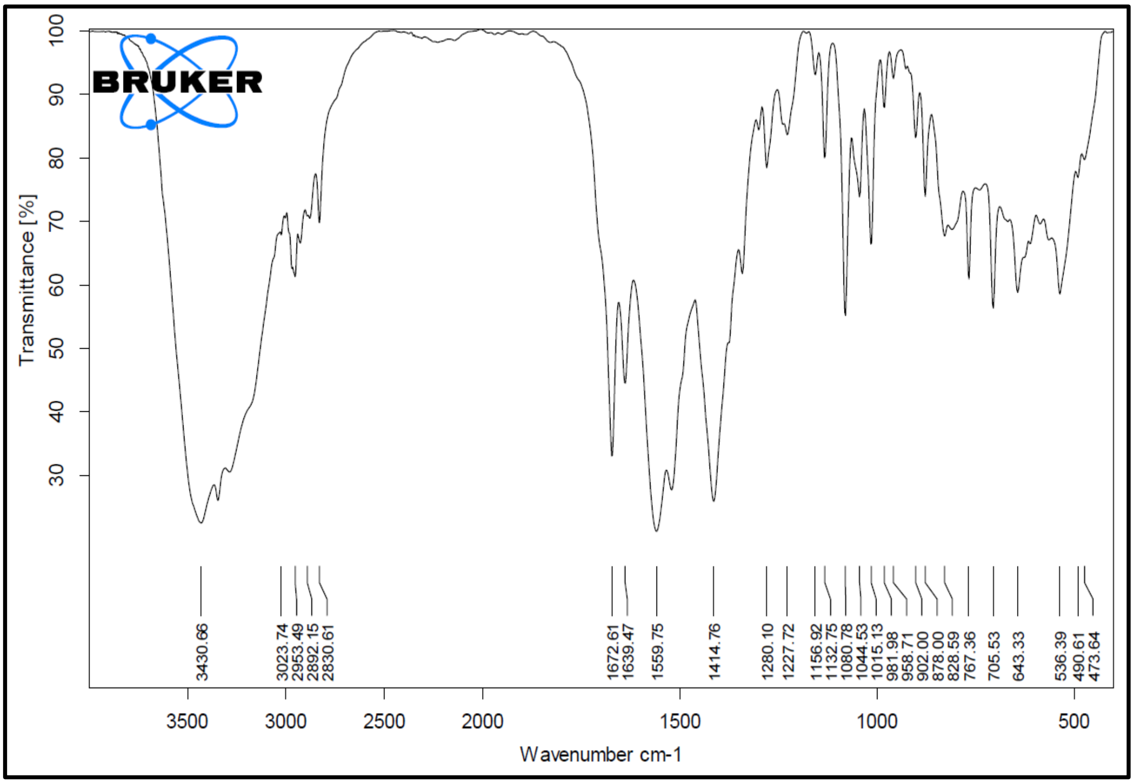

Annexure 24. IR spectrum of 9.